J. Non-Newtonian Fluid Mech. 154 (2008) 89–108

Contents lists available at ScienceDirect

Journal of Non-Newtonian Fluid Mechanics

journal homepage: www.elsevier.com/locate/jnnfm

A low Reynolds number turbulence closure for viscoelastic fluids

F.T. Pinho [a,b,*], C.F. Li [c], B.A. Younis [d], R. Sureshkumar [c]

[a] Centro de Estudos de Fenómenos de Transporte, Faculdade de Engenharia, Universidade do Porto, rua Dr. Roberto Frias s/n, 4200-465 Porto, Portugal
[b] Universidade do Minho, Largo do Paço, 4704-553 Braga, Portugal
[c] Department of Energy, Environmental and Chemical Engineering, The Center for Materials Innovation, Washington University, St. Louis, MO 63130, USA
[d] Department of Civil and Environmental Engineering, University of California, Davis, CA 95616, USA

ARTICLE INFO

Article history:
Received 2 August 2007
Received in revised form 26 February 2008
Accepted 27 February 2008
Available online xxx

Keywords:
Turbulence model
DNS
FENE-P
Drag reduction
Viscoelastic
Viscoelastic stress work

ABSTRACT

A Reynolds-averaged Navier–Stokes equation framework is developed for modeling polymer-induced turbulent drag reduction by utilizing the finitely extensible nonlinear elastic-Peterlin (FENE-P) constitutive relationship to describe fluid rheology. A self-consistent system of model equations is derived. The dominant correlations among the flow and polymer conformation variables are identified by analyzing results from recent direct numerical simulations (DNS) for dilute polymer solutions. Closures are developed for turbulent correlations that arise from viscoelasticity and incorporated into a single-point $k-\varepsilon$ model. Comparison of model predictions with DNS data obtained for an identical set of rheological and geometric parameters in the low drag reduction regime allows for a critical evaluation of the model and closure approximations. Overall, the model predictions are encouraging. This approach can be extended to higher order turbulence models and cases with higher levels of drag reduction.

1. Introduction

Viscoelastic polymer solutions, flowing under turbulent flow conditions, exhibit a significant reduction of the friction coefficient relative to the corresponding Newtonian flow. This phenomenon, referred to as turbulent drag reduction (DR), is associated with significant modification of the mean flow and the turbulence structure [1,2]. It has long been known that long, high molecular weight, flexible polymers are particularly efficient drag reducers [3,4] so that small amounts of additives result in large DRs. From a phenomenological perspective, DR has been well characterized as is evident from the comprehensive reviews of Hoyt [5] and Virk [6].

Theories on the mechanisms underlying DR abound [7–11] with recent impetus provided by the availability of results from direct numerical simulations (DNS) of turbulent channel flow with viscoelastic constitutive equations [12–16]. Most DNS studies were carried out using the finitely extensible-nonlinear-elastic model, with Peterlin's approximation (FENE-P model) [17], and were aimed at advancing the understanding of DR and its relation to the fluid rheology at high Reynolds numbers [16,18,19]. It is now generally accepted that DR is associated with increased fluid resistance due to the high extensional viscosity of the viscoelastic polymer solutions leading to a reduction in the vortex dynamic activities that are characteristic of turbulence. The crucial events take place near the wall, in the viscous and buffer sublayers, where the molecules become more extended. This is essentially in agreement with the original proposals of Metzner and Lumley [7,8]. Recently, Kim et al. [20,21] analyzed the effect of DR on coherent structures in turbulent channel flow by applying linear stochastic estimation techniques to DNS data. These studies show that polymer-induced torques counteract mechanisms central to the production of turbulence. For example the distribution of viscoelastic forces around hairpin vortices is such that they inhibit the Q2 pumping mechanism responsible for shear layer instabilities and mixing. Further, viscoelastic forces can also suppress the nonlinear autogeneration mechanism of hairpins. These findings are consistent with the mechanistic insights gained by studying the effect of elasticity on coherent structures [22,23].

While there has been much progress in DNS and coherent structure-based modeling of DR, they have certain drawbacks. DNS is extremely computationally expensive especially for high Reynolds numbers. Hence, it is impractical for industrial applications, especially for viscoelastic fluids, which solve more equations, require larger simulation boxes, smaller time steps and lengthier calculations to capture the turbulent structures than the corresponding Newtonian cases [24]. Not surprisingly, the use of DNS for viscoelastic fluids has been confined to channel/tube flows, planar boundary layers and decay of grid turbulence. Hence, modeling approaches for turbulent flow have to be developed and these are

* Corresponding author at: Centro de Estudos de Fenómenos de Transporte, Faculdade de Engenharia, Universidade do Porto, rua Dr. Roberto Frias s/n, 4200-465 Porto, Portugal.
E-mail addresses: fpinho@fe.up.pt (F.T. Pinho), bayounis@ucdavis.edu (B.A. Younis), suresh@wustl.edu (R. Sureshkumar).

0377-0257/$ – see front matter © 2008 Elsevier B.V. All rights reserved.
doi:10.1016/j.jnnfm.2008.02.008

essentially of Reynolds-averaged Navier–Stokes (RANS) type or of large eddy simulation (LES) type.

As far as we are aware, the first turbulence models for drag reducing fluids are those of [25,26] which essentially involved modifications of Newtonian models without any rheological input. An exception is the work of Mizushina and Usui [27] who based the turbulence model on the viscoelastic constitutive equation of Maxwell. Pinho [28] pointed out that all these models are based on the eddy viscosity concept and require ad-hoc, flow-dependent, modifications since they were developed without reference to fluid rheology or constitutive modeling. More recently Pinho et al. [29] developed a one-equation turbulence model which accounts for second-order viscoelastic corrections by employing closure approximations for the correlations between the fluctuations in the rate of strain and the viscoelastic stress. While such models can predict DR by suitable choice of correlation coefficients that mimic DNS data, they are strictly only applicable to small DR values (low Deborah numbers).

Turbulence models incorporating fluid rheology were proposed by Malin [30,31] and Cruz et al. [32] for power law and viscoplastic fluids devoid of elastic DR. Pinho and co-workers [28,33–36] developed some first- and second-order turbulence models, of the low Reynolds number type, in combination with a "toy" constitutive equation that integrated strain-hardening of the Trouton ratio. This enabled the prediction of both the small DR due to shear-thinning of the viscometric viscosity as well as the large DR associated with flows having large extensional viscosities. They used a special viscosity function in their generalized Newtonian model that depended on the second and the third invariants of the rate of deformation tensor, linked turbulence with the fluctuating invariant quantities appearing in the viscosity functions and incorporated these effects and the rheological parameters into the damping functions that deal with the near-wall and low Reynolds number behavior. Their low *Re* linear and nonlinear $k-\varepsilon$ turbulence models required four rheological input parameters. This enabled the correct prediction of the DR and mean velocity profiles of solutions of flexible polymers, but less well those of semi-rigid or rigid nature. The deficiencies cannot be attributed exclusively to the non-Newtonian part of the turbulence models since the original, Newtonian, closures were not asymptotically consistent at the wall. In any case, their main disadvantage was the adopted rheological constitutive equation, a toy model devoid of memory effects which requires knowledge of a fluid property that is difficult to measure namely the steady uniaxial extensional viscosity over a wide range of strain rates.

There is then a clear need to develop a turbulence closure for truly viscoelastic rheological constitutive equations that are able to model correctly the rheology of dilute and semi-dilute polymer solutions, such as the differential viscoelastic equations of Maxwell type like the Oldroyd-B, Giesekus or the FENE-P model. The required closure should also be easily parameterized with standard rheometric techniques. The FENE-P equation has been the preferred model for DNS investigations of turbulent flow of dilute polymer solutions of flexible molecules given its molecular roots [37], and there is today a wealth of DNS data enabling *a priori* development of turbulence closures. This has already been undertaken by Li et al. [38], who developed a zero equation turbulence closure for the Reynolds stresses. By its very nature this eddy viscosity model will predict very accurately some features of fully developed turbulent channel or pipe flows, or even of boundary layer flows with weak favourable pressure gradients. However, zero order models are not very successful in more complex flows given their inherent limitations [39], hence the need to develop more general eddy viscosity or Reynolds stress transport closures.

In this work we develop closures for FENE-P fluids by extending the framework of a low Reynolds number $k-\varepsilon$ turbulence model. This is done by using existing DNS data pertaining to the low DR regime. The DNS results used are those of Li et al. [24] at $Re_{\tau_0}=395$, $We_{\tau_0}=25$, $L^2=900$ and $\beta=0.9$, corresponding to a DR of 18%. The low *Re* $k-\varepsilon$ model is based on the Newtonian model of Nagano and Hishida [40], modified here to incorporate variable turbulent Prandtl numbers for the turbulent transport of k and ε as recommended by Park and Sung [41].

The paper is organized as follows: Section 2 introduces the time-average equations and identifies the viscoelastic terms requiring modeling. In Section 3, closure proposals for the viscoelastic stress work and viscoelastic turbulent transport terms are presented. The new closures are incorporated into an existing Newtonian turbulence model, which is presented in Section 4. Predictions are then obtained for fully developed turbulent channel flow and compared with the DNS data for assessment of model performance. The results, presented in Section 5, also include parametric investigations of the effects of Weissenberg number, viscosity ratio and molecular extensibility. The paper closes with a summary of the main conclusions.

2. Governing equations

The single-point turbulence model developed here is based on the time-averaged equations for viscoelastic fluids developed by Dimitropoulos et al. [42]. In what follows, upper-case letters or overbars denote time-averaged quantities and lower-case letters or primes denote fluctuating quantities. A hat denotes an instantaneous quantity.

2.1. Continuity and momentum equations

The time-averaged equations appropriate for an incompressible FENE-P fluid are:

Continuity:

$$\frac{\partial U_i}{\partial x_i}=0 \tag{1}$$

Momentum:

$$\rho\frac{\partial U_i}{\partial t}+\rho U_k\frac{\partial U_i}{\partial x_k}=-\frac{\partial \bar{p}}{\partial x_i}+\eta_s\frac{\partial^2 U_i}{\partial x_k\partial x_k}-\frac{\partial}{\partial x_k}(\rho\overline{u_iu_k})+\frac{\partial \bar{\tau}_{ik,p}}{\partial x_k} \tag{2}$$

where $\bar{\tau}_{ik,p}$ is the time-averaged polymer stress tensor, U_i is the mean velocity, $\bar{p}$ is the mean pressure, ρ is the fluid density and $-\rho\overline{u_iu_k}$ is the Reynolds stress tensor. In Eq. (2), the fluid rheology, described by the FENE-P model, introduces an extra stress which is the sum of a Newtonian solvent contribution of viscosity η_s and a polymeric contribution

$$\bar{\tau}_{ij}=2\eta_s S_{ij}+\bar{\tau}_{ij,p} \tag{3}$$

where S_{ij} is the rate of strain

$$S_{ij}=\frac{1}{2}\left(\frac{\partial U_i}{\partial x_j}+\frac{\partial U_j}{\partial x_i}\right) \tag{4}$$

Approximations are required for the time-averaged polymer stress $\bar{\tau}_{ij,p}$ and the Reynolds stress tensor $-\rho\overline{u_iu_k}$.

2.2. Rheological constitutive equation for viscoelastic fluids

To devise a model for $\bar{\tau}_{ij,p}$, we start with the instantaneous equation for the polymeric stress. For the FENE-P model (Bird et al. [17,37]), the instantaneous polymeric contribution to the total extra stress is given as an explicit function of the instantaneous

conformation tensor $\hat{C}_{ij}$

$$\hat{\tau}_{ij,\mathrm{p}} = \frac{\eta_\mathrm{p}}{\lambda}[f(\hat{C}_{kk})\hat{C}_{ij} - f(L)\delta_{ij}] \tag{5}$$

The functions $f(C_{kk})$ and $f(L)$ used here are the same as those used by Li et al. [24,38] and are given by

$$f(C_{kk}) = \frac{L^2 - 3}{L^2 - C_{kk}} \quad \text{and} \quad f(L) = 1 \tag{6}$$

Other functions are possible for the FENE-P model [43], the merits and demerits of which are discussed by Beris and Edwards [44]. It suffices to say here that the various formulations differ only for small amounts of maximum molecular extensibility L^2, which is not relevant in the context of DR, but give essentially the same results when $L^2 \gg 3$.

The conformation tensor obeys a hyperbolic differential equation of the form [37]:

$$f(\hat{C}_{kk})\hat{C}_{ij} + \lambda\left(\frac{\partial \hat{C}_{ij}}{\partial t} + \hat{U}_k\frac{\partial \hat{C}_{ij}}{\partial x_k} - \hat{C}_{jk}\frac{\partial \hat{U}_i}{\partial x_k} - \hat{C}_{ik}\frac{\partial \hat{U}_j}{\partial x_k}\right) = f(L)\delta_{ij} \tag{7a}$$

Using Eq. (5), Eq. (7a) can be alternatively written as

$$\left(\frac{\partial \hat{C}_{ij}}{\partial t} + \hat{U}_k\frac{\partial \hat{C}_{ij}}{\partial x_k} - \hat{C}_{jk}\frac{\partial \hat{U}_i}{\partial x_k} - \hat{C}_{ik}\frac{\partial \hat{U}_j}{\partial x_k}\right) = \overset{\triangledown}{\hat{C}}_{ij} = -\frac{\hat{\tau}_{ij,\mathrm{p}}}{\eta_\mathrm{p}} \tag{7b}$$

The bracketed terms in Eqs. (7a) and (7b) are the Oldroyd upper convective derivative of the instantaneous conformation tensor ($\overset{\triangledown}{\hat{C}}_{ij}$). The other parameters of the polymer constitutive equation are the relaxation time of the polymer λ and the polymer viscosity coefficient η_p.

The time-averaged polymer stress $\bar{\tau}_{ij,\mathrm{p}}$ is now given by

$$\bar{\tau}_{ij,\mathrm{p}} = \frac{\eta_\mathrm{p}}{\lambda}[f(C_{kk})C_{ij} - f(L)\delta_{ij}] + \frac{\eta_\mathrm{p}}{\lambda}\overline{f(C_{kk} + c_{kk})c_{ij}} \tag{8}$$

where the last term on the right-hand-side may also need approximation.

The time-averaged form of the conformation tensor evolution equation is

$$\overset{\triangledown}{C}_{ij} + \overline{u_k\frac{\partial c_{ij}}{\partial x_k}} - \left(\overline{c_{kj}\frac{\partial u_i}{\partial x_k}} + \overline{c_{ik}\frac{\partial u_j}{\partial x_k}}\right) = -\frac{\bar{\tau}_{ij,\mathrm{p}}}{\eta_\mathrm{p}} \tag{9a}$$

which after substitution of Eq. (8), becomes

$$\lambda\overset{\triangledown}{C}_{ij} + \lambda\left[\overline{u_k\frac{\partial c_{ij}}{\partial x_k}} - \left(\overline{c_{kj}\frac{\partial u_i}{\partial x_k}} + \overline{c_{ik}\frac{\partial u_j}{\partial x_k}}\right)\right] = -[f(C_{kk})C_{ij} - f(L)\delta_{ij} + \overline{f(C_{kk} + c_{kk})c_{ij}}] \tag{9b}$$

On the left-hand-side of Eqs. (9a) and (9b), the mean flow advective term contained within the Oldroyd derivative of C_{ij} ($\overset{\triangledown}{C}_{ij}$) is null for fully developed channel flow.

The mean flow distortion term of $\overset{\triangledown}{C}_{ij}$ is M_{ij}

$$M_{ij} = C_{kj}\frac{\partial U_i}{\partial x_k} + C_{ik}\frac{\partial U_j}{\partial x_k}$$

This is the mean flow counterpart of NLT_{ij}; it is finite, but is exact and is in no need of closure.

The remaining two terms are new and unknown. Following the analysis and nomenclature of Housiadas et al. [43] and Li et al. [38] they are labeled as

$$\mathrm{CT}_{ij} = -\overline{u_k\frac{\partial c_{ij}}{\partial x_k}}$$

which represents the contribution to the transport of the conformation tensor due to the fluctuating advective terms, and

$$\mathrm{NLT}_{ij} = \overline{c_{kj}\frac{\partial u_i}{\partial x_k}} + \overline{c_{ik}\frac{\partial u_j}{\partial x_k}}$$

which accounts for the interactions between the fluctuating components of the conformation tensor and the velocity gradient tensor. This term originates from the Oldroyd derivative and is the fluctuating counterpart of M_{ij}.

Fig. 1 shows the balance of terms in Eq. (9a) using the normalized DNS data for fully developed channel flow with DR of 18%. The results correspond to $Re_{\tau_0} = 395$, $We_{\tau_0} = 25$, $L^2 = 900$ and $\beta = 0.9$, where the Reynolds number $Re_{\tau_0} \equiv hu_\tau/\nu_0$ is based on the friction velocity (u_τ), the channel half-height (h) and the zero shear-rate kinematic viscosity of the solution, i.e., the sum of the kinematic viscosities of the solvent and polymer ($\nu_0 = \nu_\mathrm{s} + \nu_\mathrm{p}$). The Weissenberg number is $We_{\tau_0} \equiv \lambda u_\tau^2/\nu_0$ and $\beta\,(\beta \equiv \nu_\mathrm{s}/\nu_0)$ is the ratio between the solvent viscosity and the solution viscosity at zero shear-rate.

In non-dimensionalizing the variables, the velocity scale is taken to be the friction velocity (leading to the use of superscript +), the length scale is either the channel half-height ($x_i = x_i^* h$) or the viscous length ($x_i = x_i^+ \nu_0/u_\tau$), leading to superscripts * and +, respectively. When mixing the two types of normalization, using wall/viscous and physical quantities, the superscript used is *, e.g. $M_{ij} = M_{ij}^* u_\tau/h$. The conformation tensor is already in normalized form.

Housiadas et al. [43] and Li et al. [38] have shown CT_{ij}^* to be negligible, regardless of the degree of DR. Although this does not appear to be the case for the shear component CT_{xy}^* (see Fig. 1(c)), it is nevertheless neglected here as it is much smaller than the leading term in the budget. In contrast, NLT_{ij}^* is not negligible especially for the transverse normal component, and therefore its closure is one of the main tasks of this work. Apart from the wall normal component, the main contribution to the polymer stress is still due to the mean flow terms (M_{ij}^*), a reassuring point that minimizes the impact of some deficiencies in the closure for NLT_{ij}^*.

Even though the transverse normal polymer stress $\bar{\tau}_{yy,\mathrm{p}}$ does not appear in the momentum balance for fully developed channel flow, its corresponding conformation tensor component (C_{yy}) and NLT_{yy} are needed to quantify the apparent shear viscosity, given the nonlinear nature of the FENE-P equation. The expressions for the apparent shear viscosity of the FENE-P fluid in turbulent flow are presented in Appendix A.

2.3. Model for the Reynolds stresses

We adopt the Boussinesq's turbulent stress–strain relationship

$$-\rho\overline{u_i u_j} = 2\rho\nu_\mathrm{T}S_{ij} - \tfrac{2}{3}\rho k\delta_{ij} \tag{10}$$

where k is the turbulence kinetic energy and ν_T is the eddy viscosity which, following [45], is modified by a damping function f_μ to account for near-wall effects

$$\nu_\mathrm{T} = C_\mu f_\mu\frac{k^2}{\tilde{\varepsilon}} \tag{11}$$

The eddy viscosity requires knowledge of k and the modified rate of dissipation $\tilde{\varepsilon}$. The transport equations for these variables are presented next. These contain unknown terms some of which are associated with the Newtonian solvent and others, due to the viscoelastic nature of the fluid, which will be the focus of this study. Regarding the Newtonian solvent closures, we will adopt the low Reynolds number $k-\varepsilon$ model of Nagano and Hishida [40], which is a simple model that performs reasonably well in fully developed

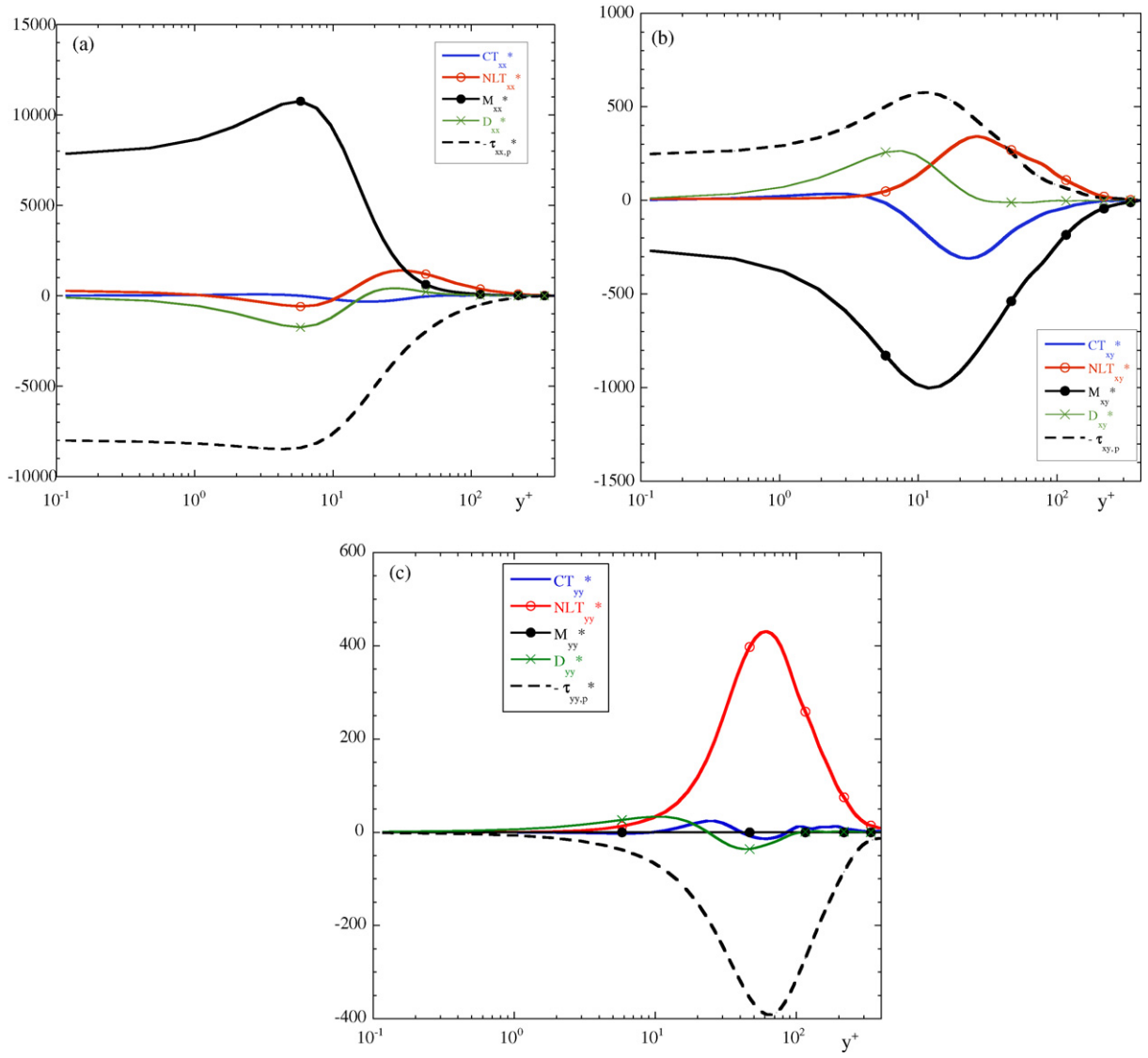

Fig. 1. Contributions to the components of the FENE-P polymer stress tensor in fully developed channel flow. DNS data for $Re_{\tau_0} = 395$, $We_{\tau_0} = 25$, $\beta = 0.9$ and $L^2 = 900$. (a) xx; (b) xy; (c) yy.

channel and pipe flows, used previously by the authors [33,34]. More recent models predict Newtonian channel flow with higher accuracy [46,47] but they introduce several new terms and damping functions which unnecessarily complicate the task of modeling the new viscoelastic terms.

2.4. Transport equation for the turbulent kinetic energy

The transport equation for the turbulent kinetic energy ($k \equiv \overline{u_i u_i}/2$) is obtained by taking the trace of the Reynolds stress transport equation (Appendix B [42]):

$$\rho \frac{Dk}{Dt} = -\rho \overline{u_i u_k} \frac{\partial U_i}{\partial x_k} - \rho \frac{\partial \overline{u_i k'}}{\partial x_i} - \frac{\partial \overline{p' u_i}}{\partial x_i} + \eta_s \frac{\partial^2 k}{\partial x_i \partial x_i} - \eta_s \overline{\frac{\partial u_i}{\partial x_j} \frac{\partial u_i}{\partial x_j}} + \frac{\partial \overline{\tau'_{ij,p} u_i}}{\partial x_j} - \overline{\tau'_{ij,p} \frac{\partial u_i}{\partial x_j}} \quad (12)$$

The term on the left-hand-side of Eq. (12) pertains to advection of k. It is exact and does not require modeling.

On the right-hand-side, the following four terms are also present in a model for Newtonian fluids:

$$P_k = -\rho \overline{u_i u_j} \frac{\partial U_i}{\partial x_j}$$

the rate of production of k. This too is exact;

$$Q_k = -\frac{\partial}{\partial x_i} (\rho \overline{u_i k'} + \overline{p' u_i})$$

the turbulent transport of k by velocity and pressure fluctuations. This is unknown and needs closure. Newtonian models of turbulent transport treat both contributions jointly. Pressure diffusion is generally negligible except perhaps near walls [48]. While it is possible that polymers can modify the pressure transport and the triple velocity correlations, departures from the Newtonian behavior are not expected to be too significant in the low DR regime. Consequently, and for the purposes of this study, turbulent transport is dealt with using a Newtonian closure.

$$D_k^N = \eta_s \frac{\partial^2 k}{\partial x_k \partial x_k}$$

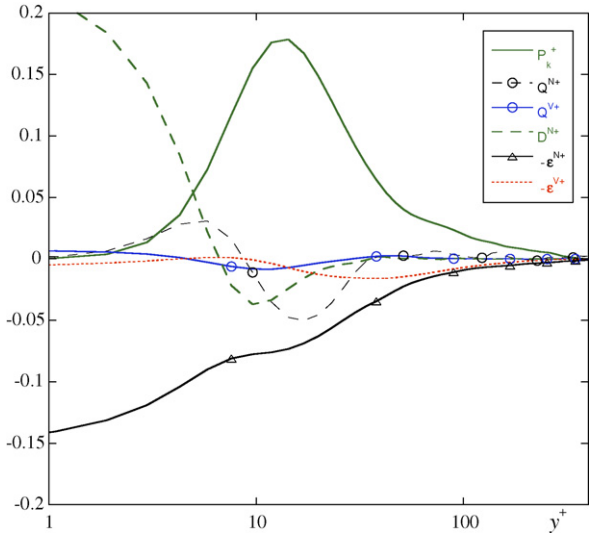

Fig. 2. Balance of turbulent kinetic energy for fully developed channel flow of a FENE-P fluid. DNS data for $Re_{\tau_0} = 395$, $We_{\tau_0} = 25$, $\beta = 0.9$ and $L^2 = 900$.

is the molecular diffusion of k associated with the Newtonian solvent which does not require closure.

$$\varepsilon^{\mathrm{N}} = \nu_{\mathrm{s}} \overline{\frac{\partial u_i}{\partial x_j} \frac{\partial u_i}{\partial x_j}}$$

is the direct viscous dissipation of k by the Newtonian solvent. This quantity is obtained from its own transport equation (Section 2.5).

Eq. (12) has two new viscoelastic terms requiring closure: the viscoelastic turbulent transport (Q^{V}) and the stress power (ε^{V}).

Using Eq. (5), Q^{V} and ε^{V} are written as (Appendix B):

$$Q^{\mathrm{V}} \equiv \frac{\partial \overline{\tau'_{ik,\mathrm{p}} u_i}}{\partial x_k} = \frac{\eta_{\mathrm{p}}}{\lambda} \frac{\partial}{\partial x_k} [C_{ik} \overline{f(C_{mm} + c_{mm}) u_i} + \overline{c_{ik} f(C_{mm} + c_{mm}) u_i}] \tag{13}$$

$$\varepsilon^{\mathrm{V}} \equiv \frac{1}{\rho} \overline{\tau'_{ik,\mathrm{p}} \frac{\partial u_i}{\partial x_k}} = \frac{\eta_{\mathrm{p}}}{\rho\lambda} \left[C_{ik} \overline{f(C_{mm} + c_{mm}) \frac{\partial u_i}{\partial x_k}} + \overline{c_{ik} f(C_{mm} + c_{mm}) \frac{\partial u_i}{\partial x_k}} \right] \tag{14}$$

The balance of turbulent kinetic energy is plotted in Fig. 2 using normalization by wall quantities (e.g. $\varepsilon = \varepsilon^+ u_\tau^4 / \nu_0$). As for a Newtonian fluid, the main contributions in the log-law region are from the production of k and the dissipation by the Newtonian solvent, with the molecular diffusion taking over the role of production well inside the viscous sublayer. The Newtonian solvent viscous dissipation is lower here than for a Newtonian fluid at the same Reynolds number (the DNS results of Mansour et al. [49] show that the maximum dissipation at the wall is of the order of 0.2, as compared to 0.15 here). Of the two viscoelastic terms the viscoelastic stress work is more important in the log-law region. The viscoelastic turbulent transport term is larger in the buffer layer and the viscous sublayer than in the log-law region. However, it remains significantly smaller than the other terms in these regions and hence deficiencies in its modeling will not have a dramatic impact on model predictions.

2.5. Transport equation for the rate of dissipation of turbulent kinetic energy

The transport equation for the rate of dissipation of k by the Newtonian solvent (ε^{N}) is derived in Appendix C. It is given as

$$\begin{aligned}
&\rho \frac{\partial \varepsilon^{\mathrm{N}}}{\partial t} + \rho U_k \frac{\partial \varepsilon^{\mathrm{N}}}{\partial x_k} \\
&= -2\eta_{\mathrm{s}} \left[\frac{\partial U_i}{\partial x_m} \overline{\frac{\partial u_i}{\partial x_m} \frac{\partial u_i}{\partial x_k}} + \frac{\partial U_i}{\partial x_k} \overline{\frac{\partial u_i}{\partial x_m} \frac{\partial u_k}{\partial x_m}} \right] - 2\eta_{\mathrm{s}} \frac{\partial^2 U_i}{\partial x_m \partial x_k} \overline{u_k \frac{\partial u_i}{\partial x_m}} \\
&\quad - 2\eta_{\mathrm{s}} \overline{\frac{\partial u_i}{\partial x_m} \frac{\partial u_i}{\partial x_k} \frac{\partial u_k}{\partial x_m}} - \frac{\partial}{\partial x_k} \left[\rho \overline{u_k \varepsilon^{\mathrm{N}'}} + 2\nu_{\mathrm{s}} \overline{\frac{\partial p'}{\partial x_m} \frac{\partial u_k}{\partial x_m}} \right] \\
&\quad + \eta_{\mathrm{s}} \frac{\partial^2 \varepsilon^{\mathrm{N}}}{\partial x_k \partial x_k} - 2\eta_{\mathrm{s}} \nu_{\mathrm{s}} \overline{\frac{\partial^2 u_i}{\partial x_m \partial x_k} \frac{\partial^2 u_i}{\partial x_m \partial x_k}} \\
&\quad + 2\nu_{\mathrm{s}} \frac{\eta_{\mathrm{p}}}{\lambda(L^2 - 3)} \overline{\frac{\partial u_i}{\partial x_m} \frac{\partial}{\partial x_m} \left\{ \frac{\partial}{\partial x_m} \left[f(C_{nn}) f(\hat{C}_{pp}) c'_{qq} C_{ik} \right] \right\}}
\end{aligned} \tag{15}$$

Compared to its Newtonian counterpart, there is an additional contribution associated with the viscoelasticity of the fluid: the last term on the right-hand-side, for which a model is required. For Newtonian fluids, only two terms in this equation are exact: the advection and the molecular diffusion of ε^{N}. The remaining terms are modeled as a function of known and calculable quantities using physical arguments, order-of-magnitude estimations and dimensional analysis [50–52].

3. Development of viscoelastic closures

3.1. Analysis of DNS data and simplifying assumptions

Closures are required for the fluctuating nonlinear term (NLT_{ij}) in the conformation tensor equation and for four terms in the balance of turbulent kinetic energy (two terms pertaining to Q^{V} and two terms pertaining to ε^{V}), viz.

$$\mathrm{NLT}_{ij} = \overline{c_{kj} \frac{\partial u_i}{\partial x_k}} + \overline{c_{ik} \frac{\partial u_j}{\partial x_k}} \tag{16a}$$

$$\overline{f(C_{mm} + c_{mm}) u_i} \quad \text{and} \quad \overline{c_{ik} f(C_{mm} + c_{mm}) u_i} \tag{16b}$$

$$\overline{f(C_{mm} + c_{mm}) \frac{\partial u_i}{\partial x_k}} \quad \text{and} \quad \overline{c_{ik} f(C_{mm} + c_{mm}) \frac{\partial u_i}{\partial x_k}} \tag{16c}$$

To develop the required closures, recourse is made to the DNS results to determine the relation between the time-averaged trace of the conformation tensor (C_{kk}) and its r.m.s. value $\left(\sqrt{\overline{c_{kk}^2}} \right)$. These quantities are plotted in Fig. 3. Near the wall, where the molecules are more stretched, the r.m.s. is approximately 25% the value of the mean value, whereas near the centerline, $\sqrt{\overline{c_{kk}^2}}$ and C_{kk} are of a similar magnitude, albeit much smaller. It is known [24] that DR is accompanied by large values of the trace of the mean conformation tensor in the buffer layer which can be more than 50% of the maximum allowed extension at large DR. We expect the same relation between the orders of magnitude of $\sqrt{\overline{c_{kk}^2}}$ and C_{kk} to hold at higher DRs where there is substantial suppression of fluctuations.

The trace of the instantaneous conformation tensor ($\hat{C}_{kk}$) appears in the function $f(\hat{C}_{kk})$ (c.f. Eq. (6)) in combination with other fluctuations leading to correlations of the type $\overline{f(C_{mm} + c_{mm}) a'}$, where a' is a fluctuating vector or tensor component. $\sqrt{\overline{c_{kk}^2}}$ is a quantity that by definition is independent of the flow direction, except perhaps very close to a wall where a preferential alignment of molecules is imposed. Since L^2 is large (in the DNS case used here $L^2 = 900$), the implication is that correlations of the type $\overline{f(C_{mm} + c_{mm}) a'}$ tend to be smaller than correlations involving two

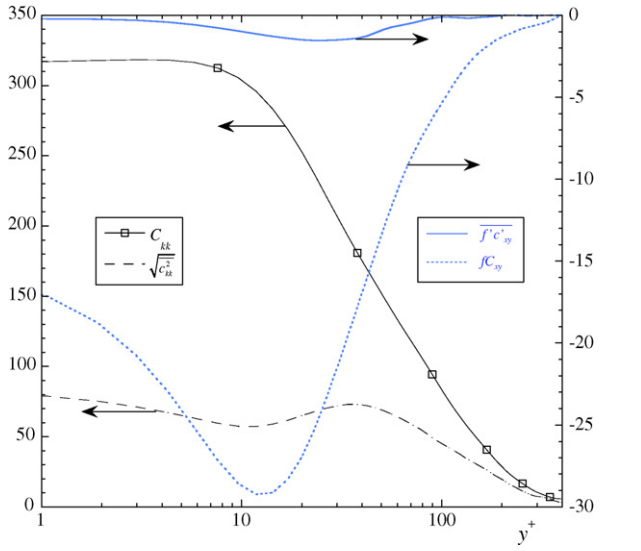

Fig. 3. DNS data of a FENE-P fluid for channel flow with DR=18% $Re_\tau = 395$, $We_\tau = 25$, $L^2 = 900$ and $\beta = 0.9$: comparison between C_{kk} and $\sqrt{\overline{c_{kk}^2}}$ (left ordinate) and between $fC_{xy} = (L^2-3)C_{xy}/(L^2 - C_{kk})$ and $\overline{f'c_{xy}} = (\overline{L^2-3})c_{xy}/(L^2 - (C_{kk} + c_{kk}))$ (right ordinate).

fluctuating quantities other than the instantaneous function $f(\hat{C}_{mm})$ (such as $\overline{f(C_{mm} + c_{mm})a'b'}$), except perhaps very close to walls. Therefore, and as a first approximation, $\overline{f(C_{mm} + c_{mm})a'}$ is neglected altogether on the grounds that it is very small in absolute terms or by comparison with the same type of term involving only mean values ($\overline{f(C_{mm} + c_{mm})a} \ll f(C_{mm})\bar{A}$). This modeling assumption is justified by the DNS results presented in Figs. 3–5.

Fig. 3 also compares $\overline{f'c_{xy}} \equiv \overline{(L^2-3)c'_{xy}/(L^2 - (C_{kk} + c'_{kk}))}$ with $f(C_{kk})C_{xy}$ (right-hand-ordinate axis). It is evident that the two have the same sign but are different by a factor of nearly 20. This confirms the assertion that, in Eq. (8), it is justifiable to neglect the last term on the right-hand-side by comparison with the first term.

Fig. 4 compares the terms in Q^V, namely $C_{iy}\overline{f'u_i} \equiv C_{iy}\overline{(L^2-3)u_i^+/(L^2 - (C_{kk} + c_{kk}))}$ with $\overline{f'c_{iy}u_i} \equiv \overline{(L^2-3)c_{iy}u_i^+/(L^2 -}$

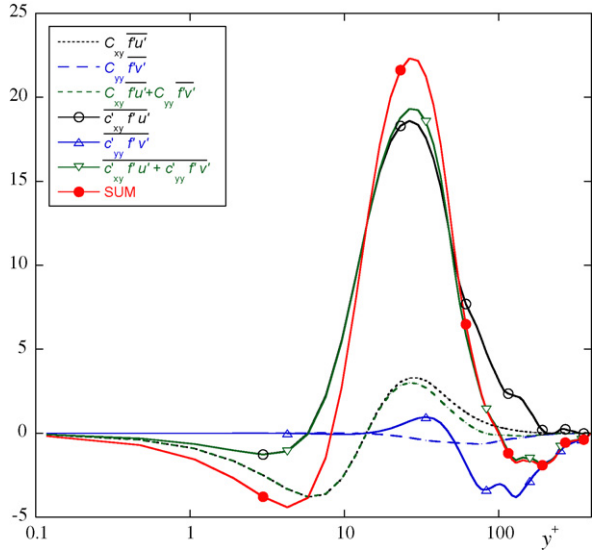

Fig. 4. Comparison between the magnitudes of $C_{iy}\overline{(L^2-3)u_i^+/(L^2 - (C_{kk} + c_{kk}))}$ and $\overline{(L^2-3)c_{iy}u_i^+/(L^2 - (C_{kk} + c_{kk}))}$ and their sum from DNS data of a FENE-P fluid for channel flow with DR = 18% ($Re_\tau = 395$, $We_\tau = 25$, $L^2 = 900$ and $\beta = 0.9$).

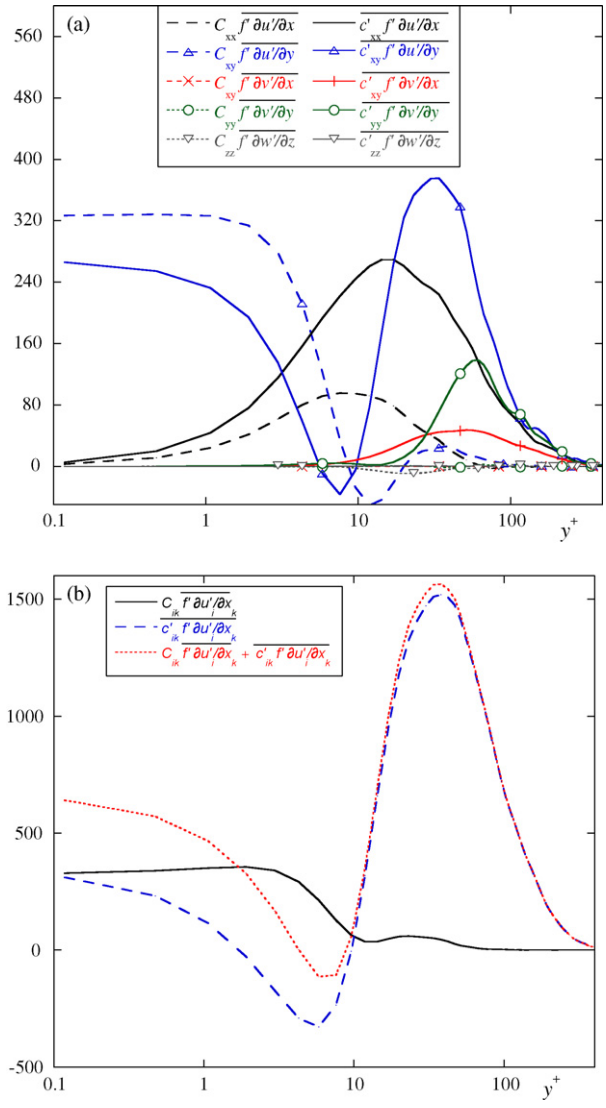

Fig. 5. Comparison between the magnitudes of individual contributions to $C_{ik}f'(C_{mm} + c'_{mm})(\partial u_i/\partial x_k)$ and $c'_{ik}f'(C_{mm} + c'_{mm})(\partial u_i/\partial x_k)$, as well as the total sums from DNS data of a FENE-P fluid for channel flow with DR=18% ($Re_\tau = 395$, $We_\tau = 25$, $L^2 = 900$ and $\beta = 0.9$). (a) Individual contributions; (b) total contributions.

$(C_{kk} + c_{kk}))$. In general, individual contributions to $C_{iy}\overline{f'u_i}$ (dashed lines) are larger than the corresponding individual contributions to $\overline{f'c_{iy}u_i}$ (full lines), except for the shear term at the junction between the viscous sublayer and the inner buffer layer, where $C_{xy}\overline{f'u'}$ is larger than $\overline{f'c_{xy}u'}$. The two terms change signs at different locations. Here too, and as a first approximation in the development of a closure for Q^V, $C_{iy}\overline{f'u_i}$ is neglected by comparison with $\overline{f'c_{iy}u'_i}$. Note that in developing a closure for $\overline{f'c_{iy}u'_i}$ by *a priori* analysis of DNS data for Q^V (plotted as SUM in Fig. 4), it is permissible to multiply the closure by a scaling coefficient to account for the neglected terms.

Fig. 5(a) compares corresponding terms in ε^V, namely individual contributions to $C_{ik}\overline{f'\partial u_i/\partial x_k}$ against individual contributions $\overline{f'c_{ik}\partial u_i/\partial x_k}$. The sums are compared in Fig. 5(b). Individual contributions to $C_{ik}\overline{f'\partial u_i/\partial x_k}$ that are not plotted are in fact zero due to symmetry considerations. From Fig. 5(a), it is evident that the contributions involving the mean conformation tensor are generally smaller than the corresponding triple correlation. The exception is $C_{xy}\overline{f'\partial u'/\partial y}$ which is larger than $\overline{c'_{xy}f'\partial u'/\partial y}$ in the viscous and buffer layers. As a consequence, in Fig. 5(b) $C_{ik}\overline{f'\partial u'_i/\partial x_k}$ is also negligible

by comparison with $\overline{c'_{ik}f'\partial u'_i/\partial x_k}$ except in the buffer and viscous sublayers. Except for this one component, individual contributions to $\overline{C_{ik}f'\partial u'_i/\partial x_k}$ can be neglected by comparison with the corresponding individual contributions to $\overline{c'_{ik}f'\partial u'_i/\partial x_k}$. While it is true that neglecting $\overline{C_{xy}f'\partial u'/\partial y}$ would significantly simplify the closure of ε^{V}, this closure would be seriously impaired in the viscous and buffer sublayers, as will be shown later. However, inspection of the balance of k^+ (c.f. Fig. 2) shows that in this region, there is a clear predominance of ε^{N} and other terms. Therefore, a discrepancy in the model for ε^{V} in the viscous and inner buffer sublayers is of no consequence, at least for low DR. For these reasons, the term $\overline{C_{xy}f'\partial u'/\partial y}$ is dropped.

The arguments put forward above and the results of Figs. 3–5 suggest that we may also safely consider the following simplification:

$$\overline{f'c_{iy}u_i} \approx f(C_{mm})\overline{c_{iy}u_i} \tag{17a}$$

$$\overline{f'c_{ik}\frac{\partial u_i}{\partial x_k}} \approx f(C_{mm})\overline{c_{ik}\frac{\partial u_i}{\partial x_k}} \tag{17b}$$

This is corroborated in Fig. 6(a) and (b). In Fig. 6(a), individual contributions to the left-hand-side of Eq. (17a) are compared with individual contributions to the right-hand-side term, including also the sums of the terms. In all cases the agreement is excellent and the small remaining differences can be accounted for with a multiplying factor whose value is close to 1. In Fig. 6(b), three sums of terms contributing to the left-hand-side of Eq. (17b) are compared with the corresponding three sums of terms on the right-hand-side, which are related to the definition of NLT_{ij}. Again the agreement is excellent and justifies the simplifications of Eqs. (17a) and (17b).

From Eqs. (17a) and (17b), the viscoelastic turbulent transport Q^{V} and the viscoelastic stress work ε^{V} simplify to

$$Q^{\mathrm{V}} \approx \frac{\eta_{\mathrm{p}}}{\lambda}\frac{\partial}{\partial x_k}[f(C_{mm})\overline{c_{ik}u_i}] = \frac{\eta_{\mathrm{p}}}{\lambda}\frac{\partial}{\partial x_k}\left[f(C_{mm})\frac{CU_{iik}}{2}\right] \tag{18}$$

$$\varepsilon^{\mathrm{V}} \approx \frac{\eta_{\mathrm{p}}}{\rho\lambda}f(C_{mm})\left[c_{ik}\frac{\partial u_i}{\partial x_k}\right] = \frac{\eta_{\mathrm{p}}}{\rho\lambda}f(C_{mm})\frac{\mathrm{NLT}_{ii}}{2} \tag{19}$$

For convenience, in Eq. (18) we define $(CU_{iik}/2) \equiv \overline{c_{ik}u_i}$, an expression originating from the more general analysis of the transport equation of the Reynolds stress tensor, where $CU_{ijk} \equiv \overline{c_{ik}u_j} + \overline{c_{jk}u_i}$. Incidentally, conclusions from order of magnitude analysis and data comparisons, and the consequent simplifications, remain applicable for second-order turbulence models where Q^{V} becomes Q^{V}_{ij} and ε^{V} becomes $\varepsilon^{\mathrm{V}}_{ij}$.

Eq. (19) is especially interesting because it shows that the closure for ε^{V} relies entirely on the closure for NLT_{ij}, reducing from 3 to 2 the number of new closures that must be developed for a FENE-P fluid. That this is a legitimate approach, and as a further confirmation of the arguments above, is seen in Fig. 7 where the two sides of Eq. (19) are compared as $\varepsilon^{\mathrm{V}+}(Re_{\tau_0})^2$ and $f(C_{mm})(\mathrm{NLT}^*_{ii}/2)$ using the normalized DNS data. Working with dimensional quantities, as in Eq. (19), indicates that the equality is only off by 7.6% at this degree of DR, i.e., the added parameter $C_{\varepsilon\mathrm{V}}$ would be of order 1. This provides further evidence that the correct physical processes can be represented by a model for ε^{V} given by

$$\varepsilon^{\mathrm{V}} = C_{\varepsilon\mathrm{V}}\frac{\eta_{\mathrm{p}}}{\rho\lambda}f(C_{mm})\frac{\mathrm{NLT}_{ii}}{2} \quad \text{with} \quad C_{\varepsilon\mathrm{V}} = 1.076 \tag{20}$$

As will be shown later, the present proposals are successful in predicting an increase in DR with L^2, but are not very sensitive to an increase in β. This highlights the urgent need to extend these closures to other Weissenberg numbers covering the low, high and maximum DR regimes.

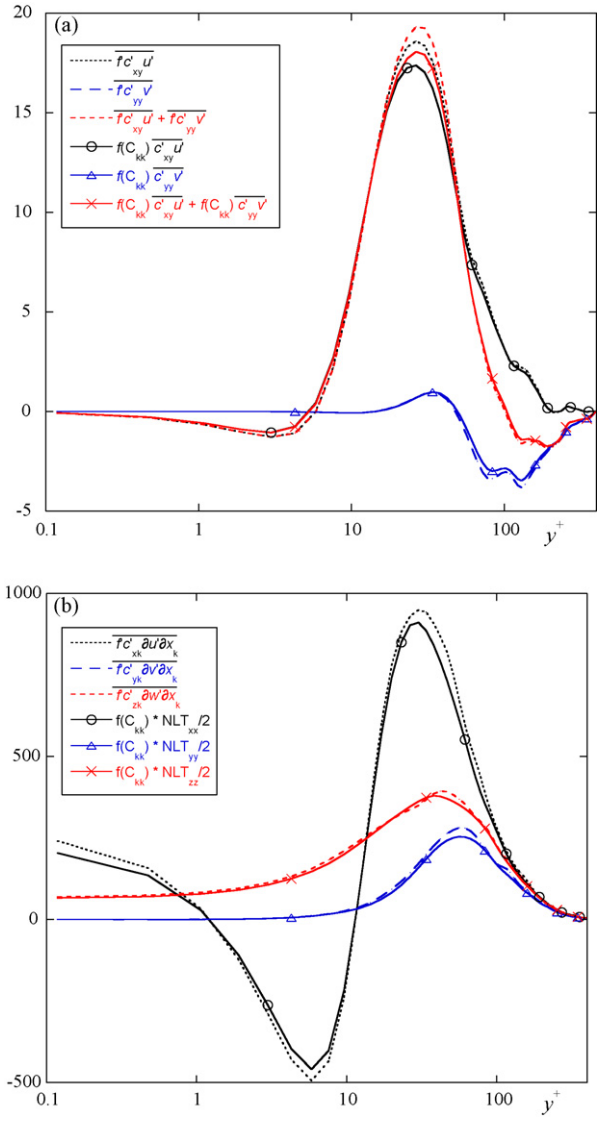

Fig. 6. Comparison between terms on the left and right-hand-sides of Eq. (17) from DNS data of a FENE-P fluid for channel flow with DR = 18% ($Re_\tau = 395$, $We_\tau = 25$, $L^2 = 900$ and $\beta = 0.9$). (a) Eq. (17a) and (b) Eq. (17b).

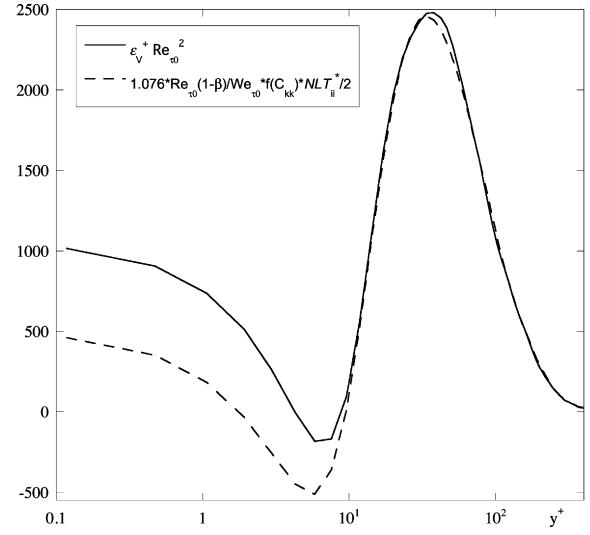

Fig. 7. Comparison between $\varepsilon^{\mathrm{V}+}Re^2_{\tau_0}$ and $f(C_{mm})\,\mathrm{NLT}^*_{ii}$ using the DNS data of FENE-P fluid in a channel flow for DR = 18% ($Re_\tau = 395$, $We_\tau = 25$, $L^2 = 900$ and $\beta = 0.9$).

3.2. Closure for NLT_{ij}

The NLT_{ij} tensor appears twice in the turbulence model: in the differential evolution equation for the conformation tensor and in the model for the viscoelastic stress work. This dual role gives NLT_{ij} an increased importance.

The exact equation for the correlation between the fluctuating conformation and velocity gradient tensors (NLT_{ij}) is derived in Pinho [53]. The equation is very complex and an alternative, simpler, expression, also derived in Pinho [53] can be obtained from Eq. (21), where NLT_{ij} is related to the quantity inside the box

$$\boxed{\overline{f\left(\hat{C}_{mm}\right)c_{kj}\frac{\partial u_i}{\partial x_k}}+\overline{f\left(\hat{C}_{mm}\right)c_{ik}\frac{\partial u_j}{\partial x_k}}}+C_{kj}\overline{f\left(\hat{C}_{mm}\right)\frac{\partial u_i}{\partial x_k}}+C_{ik}\overline{f\left(\hat{C}_{mm}\right)\frac{\partial u_j}{\partial x_k}}+\lambda\left[\overline{\frac{\partial u_i}{\partial x_k}\frac{\partial c_{kj}}{\partial t}}+\overline{\frac{\partial u_j}{\partial x_k}\frac{\partial c_{ik}}{\partial t}}\right]$$

$$+\lambda\left[\frac{\partial C_{kj}}{\partial x_n}\overline{u_n\frac{\partial u_i}{\partial x_k}}+\frac{\partial C_{ik}}{\partial x_n}\overline{u_n\frac{\partial u_j}{\partial x_k}}+\overline{\frac{\partial\left(U_n c_{kj}\right)}{\partial x_n}\frac{\partial u_i}{\partial x_k}}+\overline{\frac{\partial\left(U_n c_{ik}\right)}{\partial x_n}\frac{\partial u_j}{\partial x_k}}+\overline{u_n\frac{\partial c_{kj}}{\partial x_n}\frac{\partial u_i}{\partial x_k}}+\overline{u_n\frac{\partial c_{ik}}{\partial x_n}\frac{\partial u_j}{\partial x_k}}\right]$$

$$-\lambda\left[\frac{\partial U_k}{\partial x_n}\left(\overline{c_{jn}\frac{\partial u_i}{\partial x_k}}+\overline{c_{in}\frac{\partial u_j}{\partial x_k}}\right)+\frac{\partial U_j}{\partial x_n}\overline{c_{kn}\frac{\partial u_i}{\partial x_k}}+\frac{\partial U_i}{\partial x_n}\overline{c_{kn}\frac{\partial u_j}{\partial x_k}}+C_{kn}\left(\overline{\frac{\partial u_j}{\partial x_n}\frac{\partial u_i}{\partial x_k}}+\overline{\frac{\partial u_i}{\partial x_n}\frac{\partial u_j}{\partial x_k}}\right)\right]$$

$$-\lambda\left[C_{jn}\overline{\frac{\partial u_k}{\partial x_n}\frac{\partial u_i}{\partial x_k}}+C_{in}\overline{\frac{\partial u_k}{\partial x_n}\frac{\partial u_j}{\partial x_k}}+\overline{c_{jn}\frac{\partial u_k}{\partial x_n}\frac{\partial u_i}{\partial x_k}}+\overline{c_{in}\frac{\partial u_k}{\partial x_n}\frac{\partial u_j}{\partial x_k}}+\overline{c_{kn}\frac{\partial u_j}{\partial x_n}\frac{\partial u_i}{\partial x_k}}+\overline{c_{kn}\frac{\partial u_i}{\partial x_n}\frac{\partial u_j}{\partial x_k}}\right]=0 \tag{21}$$

Simplification of Eq. (21) is accomplished with the aid of four assumptions, two of which have already been invoked, viz. $\sqrt{\overline{c_{kk}^2}}\ll C_{kk}$ and $\overline{u_n(\partial c_{ij}/\partial x_k)}=0$ for all n and k. The further assumptions are as follows: for steady flows, the correlations involving $\partial c_{ij}/\partial t$ are null and the simplification inherent to Eq. (17b) remains applicable. With these assumptions, the expression for NLT_{ij} reduces to

$$\begin{aligned}
&f(C_{mm})\mathrm{NLT}_{ij}\\
&=f(C_{mm})\left(\overline{c_{kj}\frac{\partial u_i}{\partial x_k}}+\overline{c_{ik}\frac{\partial u_j}{\partial x_k}}\right)\\
&\cong-\lambda\left[\frac{\partial C_{kj}}{\partial x_n}\overline{u_n\frac{\partial u_i}{\partial x_k}}+\frac{\partial C_{ik}}{\partial x_n}\overline{u_n\frac{\partial u_j}{\partial x_k}}\right]-\lambda\left[\overline{\frac{\partial(U_n c_{kj})}{\partial x_n}\frac{\partial u_i}{\partial x_k}}+\overline{\frac{\partial(U_n c_{ik})}{\partial x_n}\frac{\partial u_j}{\partial x_k}}\right]\\
&\quad+\lambda\left[\frac{\partial U_k}{\partial x_n}\left(\overline{c_{jn}\frac{\partial u_i}{\partial x_k}}+\overline{c_{in}\frac{\partial u_j}{\partial x_k}}\right)+\frac{\partial U_j}{\partial x_n}\overline{c_{kn}\frac{\partial u_i}{\partial x_k}}+\frac{\partial U_i}{\partial x_n}\overline{c_{kn}\frac{\partial u_j}{\partial x_k}}\right]\\
&\quad+\lambda\left[C_{kn}\left(\overline{\frac{\partial u_j}{\partial x_n}\frac{\partial u_i}{\partial x_k}}+\overline{\frac{\partial u_i}{\partial x_n}\frac{\partial u_j}{\partial x_k}}\right)+C_{jn}\overline{\frac{\partial u_k}{\partial x_n}\frac{\partial u_i}{\partial x_k}}+C_{in}\overline{\frac{\partial u_k}{\partial x_n}\frac{\partial u_j}{\partial x_k}}\right.\\
&\quad\left.+\overline{c_{jn}\frac{\partial u_k}{\partial x_n}\frac{\partial u_i}{\partial x_k}}+\overline{c_{in}\frac{\partial u_k}{\partial x_n}\frac{\partial u_j}{\partial x_k}}+\overline{c_{kn}\frac{\partial u_j}{\partial x_n}\frac{\partial u_i}{\partial x_k}}\right]
\end{aligned} \tag{22}$$

A closure for NLT_{ij} is devised along the lines adopted by Younis et al. [54,55] whereby instead of attempting to model Eq. (22) term by term, a functional single-point relationship between NLT_{ij} and the set of parameters on which it depends is deduced and that is then reduced through the consistent application of symmetry, invariance, permutation and realizability constraints. The assumed functional relationship is

$$f(C_{mm})\frac{\mathrm{NLT}_{ij}}{\lambda}=\mathrm{func}\left(S_{ij},W_{ij},C_{ij},\varepsilon^{\mathrm{N}}_{ij},\frac{\partial\overline{u_iu_j}}{\partial x_k},\frac{\partial C_{ij}}{\partial x_k},\frac{\partial\,\mathrm{NLT}_{ij}}{\partial x_n}\right) \tag{23}$$

where W_{ij} is the mean vorticity tensor

$$W_{ij}=\frac{1}{2}\left(\frac{\partial U_i}{\partial x_j}-\frac{\partial U_j}{\partial x_i}\right) \tag{24}$$

Note that the closure does not depend explicitly on the rheological parameters L and β except for their implicit effect on the conformation tensor and hence, through flow-conformation coupling, the velocity field. Further studies are required to assess the robustness of this approach.

Various expansions of Eq. (25) were explored and the one which produced a reasonable representation of the main features of the DNS data is given by

$$\begin{aligned}
f(C_{kk})\,\mathrm{NLT}^{*}_{ij}&=f_{\mathrm{NLT}}\,We_{\tau_0}\,Re_{\tau_0}[C_{\mathrm{N1}}C_{kk}\overline{u_i^+u_j^+}+C_{\mathrm{N2}}(\overline{u_i^+u_k^+}W^+_{kn}C_{nj}\\
&\quad+\overline{u_j^+u_k^+}W^+_{kn}C_{ni}+\overline{u_k^+u_i^+}W^+_{jn}C_{nk})]
\end{aligned} \tag{25}$$

The coefficients in Eq. (2) take the values of $C_{\mathrm{N1}}=0.00035$ and $C_{\mathrm{N2}}=0.00015$. The damping function $f_{\mathrm{NLT}}=[1-\exp(-y^+/26.5)]^2$ is introduced to account for near-wall effects. These values of C_{N1} and C_{N2} appear to be very small but this is due to the normalization used for the DNS data. In fact, these coefficients, when multiplied by $We_{\tau_0}Re_{\tau_0}\approx10^4$, become of order 1.

For the prediction of fully developed turbulent channel flow in the context of a $k-\varepsilon^{\mathrm{N}}$ turbulence model, only the components NLT_{xy} and NLT_{yy} are required, together with the trace NLT_{ii}. These quantities are plotted in Fig. 8 after multiplication by $f(C_{kk})$. The variation of NLT_{ii} is especially complex due to the contribution of NLT_{xx}; it is positive in the viscous sublayer, becomes negative at the buffer layer and positive again in the log-law region where it assumes large values. The simple model proposed in Eq. (25) does not capture the behavior of NLT_{ii} close to the wall, but it does capture well its main feature which is the large positive peak. Eq. (25) also predicts the correct sign and magnitude of all other components of NLT_{ij}, as seen in Fig. 8. More specifically, it broadly captures the general trends of NLT_{xy} and NLT_{yy}.

A second argument for using the closure of Eq. (25) is related to the base turbulence model. The development of this closure relies on DNS data, but the closure will be used as part of a $k-\varepsilon^{\mathrm{N}}$ model, which has simplifying assumptions and some deficiencies, such as the isotropy of Reynolds stresses or the failure to predict a peak ε^{N} at the wall. Hence, even a perfect closure for NLT_{ij} would fail to predict correctly this quantity in the turbulence model. This calls for a second phase of adjustment of the closure, in Section 4 of this paper, in strict connection with the specific Newtonian base turbulence model adopted.

3.3. Closure for CU_{ijk}

The exact equation of CU_{ijk} was also derived by Pinho [53]. It is given as

$$\boxed{\overline{f\left(\hat{C}_{mm}\right)u_i c_{kj}} + \overline{f\left(\hat{C}_{mm}\right)u_j c_{ik}}} + \overline{f\left(\hat{C}_{mm}\right)u_j}C_{ik} + \overline{f\left(\hat{C}_{mm}\right)u_i}C_{kj} + \lambda\left[\overline{u_i\frac{\partial c_{kj}}{\partial t}} + \overline{u_j\frac{\partial c_{ik}}{\partial t}}\right]$$
$$+\lambda\left[\overline{u_i\frac{\partial\left(U_m c_{kj}\right)}{\partial x_m}} + \overline{u_j\frac{\partial\left(U_m c_{ik}\right)}{\partial x_m}} + \overline{u_i u_m\frac{\partial c_{kj}}{\partial x_m}} + \overline{u_j u_m\frac{\partial c_{ik}}{\partial x_m}} + \overline{u_i u_m}\frac{\partial C_{kj}}{\partial x_m} + \overline{u_j u_m}\frac{\partial C_{ik}}{\partial x_m}\right]$$
$$-\lambda\left[\left(\overline{u_j c_{im}} + \overline{u_i c_{jm}}\right)\frac{\partial U_k}{\partial x_m} + \overline{u_i c_{km}}\frac{\partial U_j}{\partial x_m} + \overline{u_j c_{km}}\frac{\partial U_i}{\partial x_m} + C_{km}\overline{\frac{\partial u_i u_j}{\partial x_m}} + C_{jm}\overline{u_i\frac{\partial u_k}{\partial x_m}} + C_{im}\overline{u_j\frac{\partial u_k}{\partial x_m}}\right]$$
$$-\lambda\left[\overline{u_i c_{jm}\frac{\partial u_k}{\partial x_m}} + \overline{u_j c_{im}\frac{\partial u_k}{\partial x_m}} + \overline{c_{km}\frac{\partial\left(u_j u_i\right)}{\partial x_m}}\right] = 0 \tag{26}$$

CU_{ijk}, defined as $\overline{u_i c_{kj}} + \overline{u_j c_{ik}}$, is related to the quantity inside the box.

Pinho [53] also simplified this equation by invoking the same assumptions used to simplify the exact equation of NLT_{ij}, except that Eq. (17a) was used instead of Eq. (17b). The first two terms on the right of the boxed terms of Eq. (26) were retained because even though $\overline{f(\hat{C}_{mm})u_j}$ is small, it multiplies a large tensor C_{ik}. The result is

$$f(C_{mm})CU_{ijk} = -\lambda\left[\overline{u_i u_m\frac{\partial c_{kj}}{\partial x_m}} + \overline{u_j u_m\frac{\partial c_{ik}}{\partial x_m}} + \overline{u_i u_m}\frac{\partial C_{kj}}{\partial x_m} + \overline{u_j u_m}\frac{\partial C_{ik}}{\partial x_m} + \overline{u_i\frac{\partial\left(U_m c_{kj}\right)}{\partial x_m}} + \overline{u_j\frac{\partial\left(U_m c_{ik}\right)}{\partial x_m}}\right]$$
$$+\lambda\left[\left(\overline{u_j c_{im}} + \overline{u_i c_{jm}}\right)\frac{\partial U_k}{\partial x_m} + \overline{u_i c_{km}}\frac{\partial U_j}{\partial x_m} + \overline{u_j c_{km}}\frac{\partial U_i}{\partial x_m}\right]$$
$$+\lambda\left[C_{km}\overline{\frac{\partial u_i u_j}{\partial x_m}} + C_{jm}\overline{u_i\frac{\partial u_k}{\partial x_m}} + C_{im}\overline{u_j\frac{\partial u_k}{\partial x_m}}\right]$$
$$+\lambda\left[\overline{u_i c_{jm}\frac{\partial u_k}{\partial x_m}} + \overline{u_j c_{im}\frac{\partial u_k}{\partial x_m}} + \overline{c_{km}\frac{\partial\left(u_j u_i\right)}{\partial x_m}}\right]$$
$$-\overline{f(\hat{C}_{mm})u_j}C_{ik} - \overline{f(\hat{C}_{mm})u_i}C_{kj} \tag{27}$$

In contrast to NLT_{ij}, the closure developed for CU_{ijk} was partially based on the reduction of Eq. (27) after decoupling some of its triple correlations into double or lesser correlations of known quantities leading to the following general expression:

$$f(C_{mm})\frac{CU_{ijk}}{\lambda} = -C_{\beta_1}\left(\overline{u_i u_m}\frac{\partial C_{kj}}{\partial x_m} + \overline{u_j u_m}\frac{\partial C_{ik}}{\partial x_m}\right) + C_{\beta_2}U_m\frac{\partial CU_{ijk}}{\partial x_m}$$
$$+C_{\beta_3}\left[\left(\overline{u_j c_{im}}+\overline{u_i c_{jm}}\right)\frac{\partial U_k}{\partial x_m}+\overline{u_i c_{km}}\frac{\partial U_j}{\partial x_m}+\overline{u_j c_{km}}\frac{\partial U_i}{\partial x_m}\right]$$
$$+C_{\beta_4}C_{km}\frac{\partial\overline{u_i u_j}}{\partial x_m} + C_{\beta_5}C_{jm}\frac{\partial\overline{u_i u_k}}{\partial x_m} + C_{\beta_6}C_{im}\frac{\partial\overline{u_j u_k}}{\partial x_m}$$
$$-\frac{C_{\beta_7}}{\lambda}f(C_{mm})\left[\pm\sqrt{\overline{u_j^2}}C_{ik} \pm \sqrt{\overline{u_i^2}}C_{jk}\right] \tag{28}$$

In modeling the last term as $\overline{f(\hat{C}_{mm})u_j}C_{ik} + \overline{f(\hat{C}_{mm})u_i}C_{kj} \approx \beta_7 f(C_{mm})\left[\pm\sqrt{\overline{u_j^2}}C_{ik} + \pm\sqrt{\overline{u_i^2}}C_{jk}\right]$ the $\pm$ sign was introduced to ensure that the correct sign of the model is obtained given that the approach adopted here assumes positive values for the double correlation. For a velocity component normal to a symmetry plane, the double correlation is anti-symmetric and this property must be kept in the closure. In Eq. (28) note also that $\overline{u_j c_{im}} + \overline{u_i c_{jm}} \equiv CU_{ijm}$.

The general model proposed in Eq. (28) is Galilean-invariant, invariant with respect to rotations and reflections of the coordinate system. A simpler model is obtained by retaining only the two leading terms of Eq. (28). This is given as

$$f(C_{mm})CU^+_{ijk} = -f_{CU}\left\{C_{\beta_1}\frac{We_{\tau_0}}{Re_{\tau_0}}\left(\overline{u_i u_m^+}\frac{\partial C_{kj}}{\partial x_m^*} + \overline{u_j u_m^+}\frac{\partial C_{ik}}{\partial x_m^*}\right)\right.$$
$$\left.+C_{\beta_7}f(C_{mm})\left[\pm\sqrt{\overline{u_j^{+2}}}C_{ik} \pm \sqrt{\overline{u_i^{+2}}}C_{jk}\right]\right\} \tag{29}$$

The coefficients of the model take the values $C_{\beta_1} = 1.3$ and $C_{\beta_7} = 0.37$.

Fig. 9 shows a comparison between this model and the DNS results for the quantity appearing in the viscoelastic turbulent

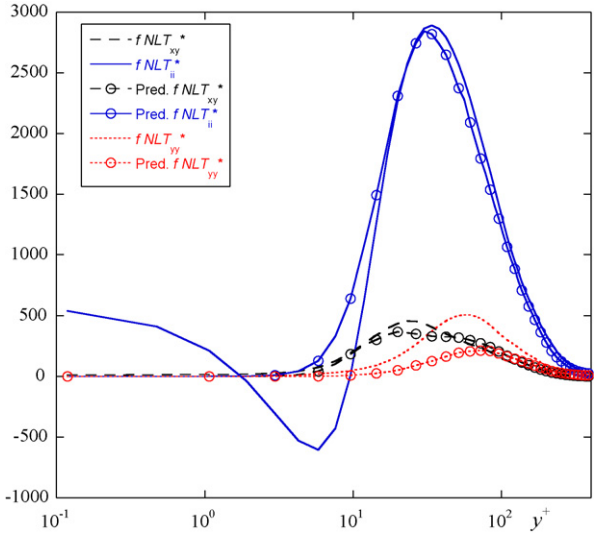

Fig. 8. Comparison between DNS data for fully developed channel flow of FENE-P fluid ($Re_\tau = 395$, $We_\tau = 25$, $L^2 = 900$ and $\beta = 0.9$) for some components of $f(C_{kk})NLT^*_{ij}$ with the predictions of Eq. (25).

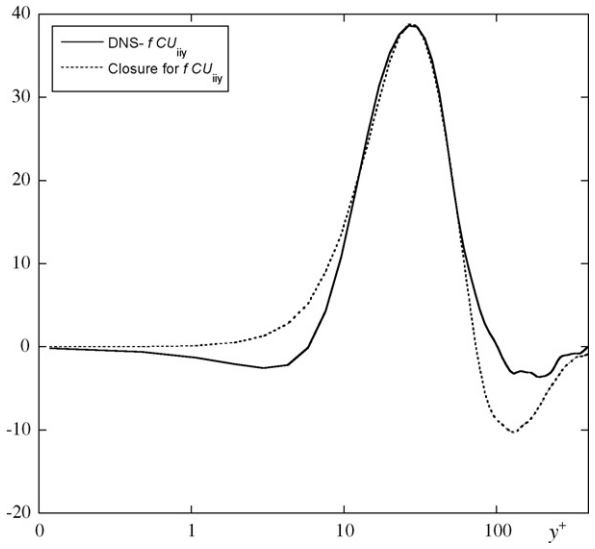

Fig. 9. Comparison between DNS data for fully developed channel flow of FENE-P fluid ($Re_\tau = 395$, $We_\tau = 25$, $L^2 = 900$ and $\beta = 0.9$) for $f(C_{kk})CU^+_{iiy}$ with the predictions of Eq. (29).

transport of k. The main features of CU_{iiy} are well captured by Eq. (29). To comply with the damping effect of the wall, and to match the predictions of the model with the DNS data, it was necessary to introduce a damping function $f_{CU} = 1 - \exp(-y^+/26.5)$.

The viscoelastic turbulent transport Q^V is actually the derivative of $f(C_{kk})CU_{iiy}$ and so the essential characteristic of this quantity is the positive peak for $y^+ > 10$. The DNS data for DR = 18% also show a region close to the wall with slight negative values of $f(C_{kk})CU^+_{iiy}$ and a small, but sharp negative peak near the centreline. Whereas the former is not captured by the proposed closure, the latter is overpredicted, both features requiring future improvements.

For the present purpose, the main peak is the essential feature of the flow, and its magnitude and location are well captured by this closure.

4. Turbulence model

The closures developed in Section 3 were incorporated into a modified version of the low Reynolds number $k-\varepsilon^N$ model of Nagano and Hishida [40] for Newtonian fluids utilizing variable turbulent Prandtl numbers for k and ε [41–46].

The time-averaged polymer stresses which appear in the momentum equations (Eq. (2)) are obtained from

$$\bar{\tau}_{ij,p} = \frac{\eta_p}{\lambda}[f(C_{kk})C_{ij} - f(L)\delta_{ij}] \tag{30}$$

The conformation tensor in Eq. (30) is obtained from

$$\lambda(\overset{\nabla}{C}_{ij} - \mathrm{NLT}_{ij}) = -[f(C_{kk})C_{ij} - f(L)\delta_{ij}] \tag{31}$$

The Reynolds stress is given by Boussinesq's stress–strain relationship (Eq. (10)). The eddy viscosity which appears in this equation differs from the original coefficient for Newtonian fluids in that it includes the total dissipation of turbulent kinetic energy, not just the dissipation by the solvent (ε^N):

$$\nu_T = C_\mu f_\mu \frac{k^2}{\tilde{\varepsilon}^N + \varepsilon^V} \tag{32}$$

The damping function f_μ remains the same as for a Newtonian fluid.

The turbulent kinetic energy is obtained from the equation:

$$\frac{\partial \rho k}{\partial t} + \frac{\partial \rho U_i k}{\partial x_i} = -\rho\overline{u_i u_k}\frac{\partial U_i}{\partial x_k} + \frac{\partial}{\partial x_i}\left[\left(\eta_s + \frac{\rho f_t \nu_T}{\sigma_k}\right)\frac{\partial k}{\partial x_i}\right] + \eta_s \frac{\partial^2 k}{\partial x_i \partial x_i} - \rho\tilde{\varepsilon}^N - \rho D + \frac{\eta_p}{\lambda}\frac{\partial}{\partial x_i}\left[f(C_{mm})\frac{CU_{kki}}{2}\right] - \frac{\eta_p}{\lambda}f(C_{mm})\frac{\mathrm{NLT}_{kk}}{2} \tag{33}$$

Here, the modified rate of dissipation $\tilde{\varepsilon}^N$ is used as is often the case in low Reynolds number models. It differs from the true dissipation ε^N very close to walls and is given by $\varepsilon^N = \tilde{\varepsilon}^N + D$, where D is defined as

$$D = 2\nu_s\left(\frac{d\sqrt{k}}{dy}\right)^2 \tag{34}$$

The transport equation for the modified rate of dissipation is

$$\frac{\partial \rho\tilde{\varepsilon}^N}{\partial t} + \frac{\partial \rho U_i \tilde{\varepsilon}^N}{\partial x_i} = \frac{\partial}{\partial x_i}\left[\left(\eta_s + \frac{\rho f_t \nu_T}{\sigma_\varepsilon}\right)\frac{\partial \tilde{\varepsilon}^N}{\partial x_i}\right] + f_1 C_{\varepsilon_1}\frac{\tilde{\varepsilon}^N}{k}P_k - f_2 C_{\varepsilon_2}\rho\frac{\tilde{\varepsilon}^{N2}}{k} + \rho E + E_{\tau_p} \tag{35}$$

where the production of turbulent kinetic energy is $P_k = -\rho\overline{u_i u_j}(\partial U_i/\partial x_j)$, $E = \nu_s \nu_T (1-f_\mu)(\partial^2 U_i/\partial y \partial y)^2$ and E_{τ_p} is the last term on the right-hand-side of Eq. (15), due to the presence of the viscoelastic fluid, which is here taken as $E_{\tau_p} = 0$. The damping functions are $f_\mu = [1 - \exp(-y^+/26.5)]^2$, with $y^+ = u_\tau y/\nu_{wall}$ based on the wall viscosity of the solution, $f_1 = 1.0$ and $f_2 = 1 - 0.3\exp(-R_T^2)$ with $R_T = k^2/(\nu_s\tilde{\varepsilon}^N)$.

NLT_{ij}, and consequently NLT_{kk} in Eq. (33), is given by Eq. (25) with $C_{N1} = 0.00035$ and $C_{N2} = 0.00015$ and $f_{NLT} = f_\mu$. CU_{iiy} is calculated from Eq. (29) with $C_{\beta_1} = 1.3$ and $C_{\beta_7} = 0.37$ and $f_{CU} = \sqrt{f_\mu}$. As already mentioned in Section 3.2, the small numerical values of C_{N1} and C_{N2} are related to the way Eq. (25) is normalized. When multiplied by We_{τ_0} and Re_{τ_0} (c.f., Eq. (25)) the coefficients become 3.5 and 1.5, respectively.

Using in the turbulence model the value of C_{N1} obtained in the model calibration against DNS data, $C_{N_1} = 0.00035$, results in overestimation of NLT_{ij} and significantly larger DRs than observed. In the second phase of the development of the viscoelastic closure, this parameter was reduced in order to match the DR and the same values of $Re_{\tau_0} = 395$ and $We_{\tau_0} = 25$, to which corresponds DR = 18%, while keeping unchanged the other coefficient of NLT_{ij}. Regarding CU_{iiy}, using the original values of C_{β_1} and C_{β_7} also resulted in an over-prediction of CU_{iiy}, but its impact on other quantities was small. These two coefficients were also reduced for improved model performance.

The remaining parameters in the model are assigned their usual values, i.e., $C_\mu = 0.09$, $C_{\varepsilon_1} = 1.45$ and $C_{\varepsilon_2} = 1.90$. Regarding the turbulent Prandtl numbers for k and ε, two combinations are used: the original set of Nagano and Hishida [40] with $\sigma_k = 1.0$ and $\sigma_\varepsilon = 1.3$, and the set recommended by Nagano and Shimada [46] and Park and Sung [41] to increase turbulent diffusion in the near-wall region while reducing it far from the wall. This second set uses $\sigma_k = 1.1$ and $\sigma_\varepsilon = 1.3$ together with the function f_t:

$$f_t = 1 + 3.5\exp[-(R_T/150)^2] \tag{36}$$

5. Results and discussion

Three sets of results are presented and analyzed separately in this section. In Section 5.1 six variants of the proposed closures are

Table 1
Numerical values of some parameters used in the viscoelastic simulations for $Re_{\tau_0} = 395$, $We_{\tau_0} = 25$, $L^2 = 900$ and $\beta = 0.9$

	C_{N1}	C_{β_1}	C_{β_7}	σ_k	σ_ε	ε^V
Run 1	0.000277	1.3	0.37	1.0	1.3	No
Run 2	0.000291	1.3	0.37	1.1 & f_t	1.3 & f_t	No
Run 3	0.000293	0.65	0.18	1.1 & f_t	1.3 & f_t	No
Run 4	0.000266	0.65	0.18	1.1 & f_t	1.3 & f_t	Yes
Run 5	0.000270	0.65	0.18	1.0	1.3	Yes
Run 6	0.000266	0.754	0.215	1.1 & f_t	1.3 & f_t	Yes

f_t refers to the use of a variable Prandtl number via f_t of Eq. (36), otherwise $f_t = 1$. ε^V refers as to whether or not ε^V is used in the definition of ν_T in Eq. (32).

assessed by comparison with one set of DNS data pertaining to the low DR regime. Then, in Section 5.2 two sets of results are presented to assess the performance of one of the models by looking at the effects of Weissenberg number, L^2 and β. These comparisons allow a critical evaluation of the various closures proposed.

5.1. Model performance against DNS data

In this section, results from several simulations are presented. Unless otherwise stated, the DNS results pertain to $Re_{\tau_0} = 395$ and, for the viscoelastic fluids, for rheological parameters given by $We_{\tau_0} = 25$, $L^2 = 900$ and $\beta = 0.9$ which corresponds to a DR of 18%. All viscoelastic flow calculations were carried out using the same channel dimensions and bulk velocity as the DNS. Simulations were performed to assess the effect of the variations in the coefficients present in the turbulence model on DR predictions (see Table 1). This amounts to testing different turbulence models in order to select the best based on the general closures of Sections 3.2–3.4. In all cases, the coefficient C_{N_1} was changed to match the DNS values of Re_{τ_0} and We_{τ_0}. The numerical simulations were carried out with the finite-volume code of Younis [56] adapted for the FENE-P fluid by Pinho and co-workers [33–36]. Non-uniform meshes of 99 cells across the channel were used with at least 8 cells located within each of the viscous sublayers. This computational grid gives mesh independent results within 0.5% for the mean velocity profile and the friction factor.

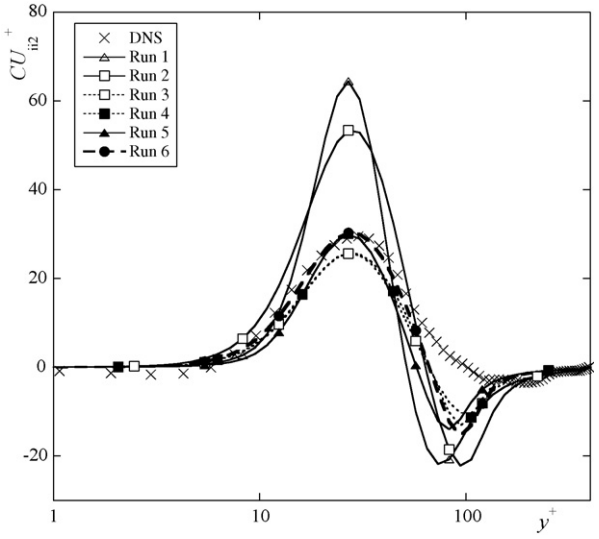

Fig. 11. Normalised CU_{iiy} in wall coordinates. Comparison between DNS and predictions (runs 1–6 of Table 1) for FENE-P fluids in turbulent channel flow.

As shown in Table 1, σ_k and σ_ε were taken as constant in runs 1 and 5, but as variable for runs 2–4. Another difference concerns the use of ε^V in the definition of ν_T (c.f. Eq. (32)) for runs 4–6 in contrast to the classical Newtonian definition used in runs 1–3. The third difference is in the numerical values of parameters C_{β_1} and C_{β_7}, i.e., in the model predictions of CU_{kky}.

Fig. 10 compares the predicted and DNS results for mean velocity profiles in wall coordinates for DR = 18%. The Newtonian profile at the same Reynolds number is also shown. It is clear that the viscoelastic simulations capture DR of an extent which is very close to the DNS, especially for constant σ_k and σ_ε. The use of variable Prandtl numbers reduces the slope of the mean velocity in the buffer layer, but it is nevertheless recommended by Nagano and Shimada [46] and Park and Sung [41] as it improves predictions of other quantities such as the turbulence kinetic energy and its rate of dissipation. Run 1 slightly overpredicts run 5, these two simulations differ in the viscoelastic turbulent transport model coefficients. All

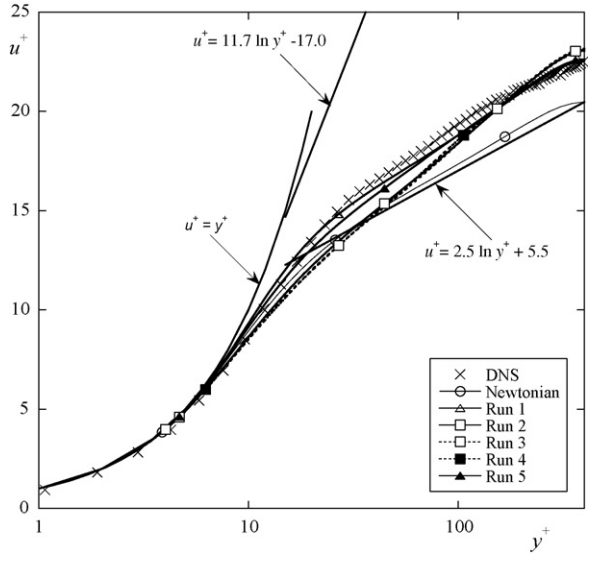

Fig. 10. Comparison between DNS data for FENE-P fluid in turbulent channel flow and the corresponding predictions for runs 1–5 of Table 1. Mean velocity profile normalized in wall coordinates. Includes Newtonian fluid prediction.

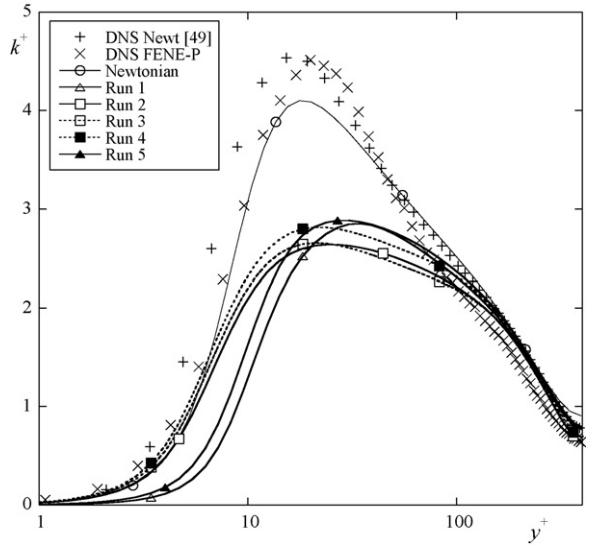

Fig. 12. Turbulent kinetic energy in wall coordinates. Comparison between DNS data for Newtonian (from Mansour et al. [49]) and FENE-P fluids in turbulent channel flow and the corresponding Newtonian and FENE-P predictions (runs 1–5 of Table 1).

simulations underpredict the DNS in the buffer layer and in the log-law region, but cross over the DNS data as the centerline is approached, because of mass conservation. Making the eddy viscosity depend directly on the viscoelastic stress work has little impact on the mean velocity, but improves the prediction of other quantities as will be seen later. In any case, as far as the mean velocity is concerned, and apart from the variable Prandtl numbers σ_k and σ_ε, other modeling differences have a small impact.

The predicted and DNS profiles of CU_{kky} are shown in Fig. 11. The use of the original values of the parameters C_{β_1} and C_{β_7} in runs 1 and 2, which produced reasonably good agreement between the closure and the DNS in Fig. 9, results in overprediction of CU_{kky} when this closure is used in the $k-\varepsilon^{\mathrm{N}}$ turbulence model. This difference is a consequence of the limitations of the $k-\varepsilon^{\mathrm{N}}$ model especially in terms of its predictions of quantities like the Reynolds stresses and its gradients. If these behave quantitatively differently in the predictions compared to the DNS used to derive the closures, then these closures will give a different result in the model, which then changes further the predicted quantities in a feedback cycle. An example is the Reynolds stresses, which are anisotropic, but are taken as isotropic in this $k-\varepsilon^{\mathrm{N}}$ model. Hence, it was necessary to reduce the values of C_{β_1} and C_{β_7} in order to be able to predict the correct peak value of CU_{kky}. Using variable Prandtl numbers improves also the prediction of CU_{kky}, especially in the buffer layer. Better prediction of this quantity was obtained in run 6, where C_{β_1} and C_{β_7} were increased. Nevertheless, in all cases the predicted distribution of CU_{kky} tends to be sharper and the negative peak in the inertial layer is also over-predicted. For conciseness, only data from run 6 is shown in this figure.

As can be seen from Fig. 12, the predicted turbulent kinetic energy does not follow the trends in the DNS. The profile of k^+ for DR = 18% is actually not too different from the DNS profile of Mansour et al. [49] for a Newtonian fluid at the same Reynolds number, and the predicted Newtonian profile is similar to these two DNS profiles. However, the inclusion of viscoelasticity reduces significantly the predicted values of k^+. The use of the variable σ_k and σ_ε (via f_t) generally improves the predictions of k close to the wall and it is clear that the best predictions of k combine this feature with lower values of C_{β_1} and C_{β_7} for improved prediction of CU_{kky} and the use of ε^{V} to define ν_{T}.

Drag reduction is associated with a decrease in the Reynolds shear stress. By adopting the Prandtl–Kolmogorov model for the eddy viscosity, this reduction can be achieved via a decrease in k alone or in combination with an increase in $\varepsilon^{\mathrm{N}+}$. Since $\varepsilon^{\mathrm{N}+}$ is also reduced, as will be shown shortly, the DR must be accompanied by a larger decrease in k, which will then be underpredicted. Further development of the model is needed to address this issue to improve the predictions of k and ε^{N} while giving the correct DR and the correct Reynolds shear stress profiles, as shown in Fig. 13(a). The expected decrease in $\overline{u'v'}^+$ is captured by the present turbulence model but the extent of reduction is overestimated. These variations in $\overline{u'v'}^+$ should come together with different predictions of the normalized polymer stresses (the Newtonian solvent stresses are not expected to be too different since the velocity gradients are practically unaffected by DR). Hence, the lower peak values of the predicted $\overline{u'v'}^+$, and especially for runs 3 and 4, are accompanied by an overprediction of the polymer stress, as can be seen in Fig. 13(b) where the three relevant shear stresses are plotted for run 4. The

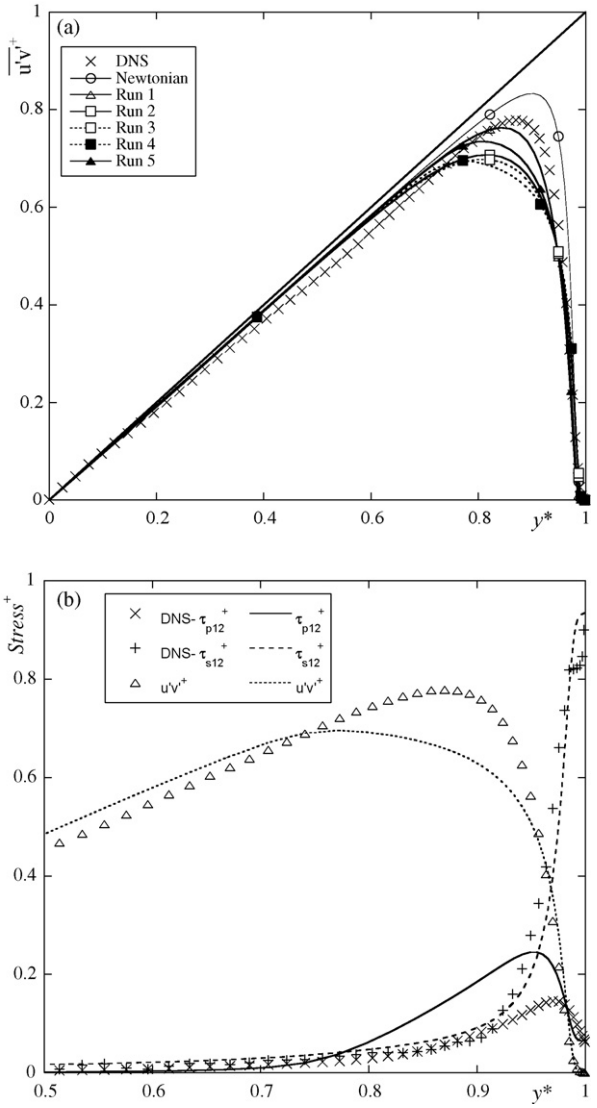

Fig. 13. Normalized shear stresses. Comparison between DNS data for FENE-P fluid in turbulent channel flow and the corresponding predictions (runs 1–5 of Table 1 and Newtonian prediction). (a) Comparison between Reynolds shear stress; (b) comparison between Reynolds stress, polymer stress and solvent stress for run 4.

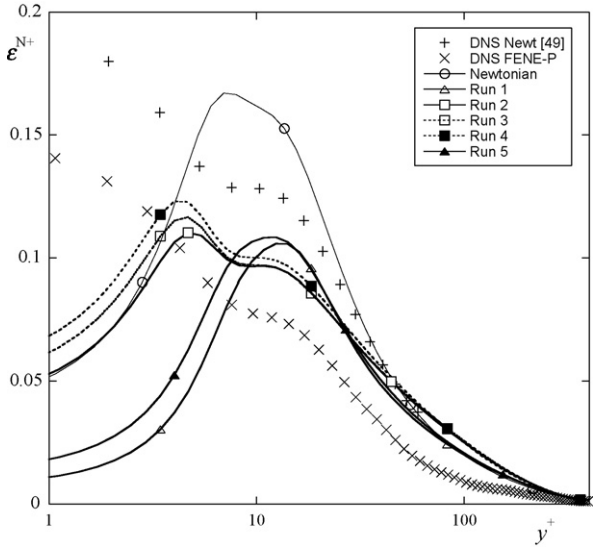

Fig. 14. Normalized Newtonian solvent rate of dissipation of k in wall coordinates. Comparison between DNS data for Newtonian ($Re_\tau = 395$ from Mansour et al. [49]) and FENE-P fluid in turbulent channel flow and the corresponding Newtonian and FENE-P predictions (runs 1–5 of Table 1).

interplay between the Reynolds and polymer stress is clear in this plot, whereas the solvent shear stress is well predicted and shows no appreciable variation from run to run.

The predictions and simulations of ε^{N+} are compared in Fig. 14. Runs 1 and 5 (with constant σ_k and σ_ε) exhibit a peak ε^{N+} at $y^+ \approx 10$, whereas the remaining runs, with variable σ_k and σ_ε, show the characteristic plateau in this region followed by a further increase of ε^{N+} towards the wall. In all cases, very close to the wall, ε^N decreases to a finite value, in contrast to the correct behavior. This defect is related to the Newtonian base turbulence model and requires a more sophisticated modeling approach [41,57]. Indeed, the DNS profile of ε^{N+} from Mansour et al. [49] for Newtonian channel flow has a similar shape to the DNS profile of ε^{N+} for the FENE-P fluid, but the former is consistently higher with a maximum value of ε^{N+} of around 0.2 (in normalized quantities) against around 0.15. The viscoelastic predictions of the solvent dissipation ε^{N+} are all lower than for the pure Newtonian fluid, but higher than the viscoelastic DNS. This is unexpected but is again related to the deficiencies of the Nagano and Hishida [40] formulation in predicting the rate of dissipation and indicates the need for improvement of the base turbulence model. Such improvement is usually obtained via corrections to the modeled transport equation of ε^N, as well as by the use of more elaborate damping functions [46,57].

The predictions of NLT^*_{kk}, NLT^*_{yy} and NLT^*_{xy} are shown in Fig. 15(a)–(c). As expected, in all cases the predicted shapes are similar, but there are some differences from the DNS. Both NLT^*_{kk} and NLT^*_{xy} are underpredicted by about 60%, whereas NLT^*_{yy} is well predicted in magnitude but the profile is shifted towards lower values of y^+. These differences are associated with lower values of C_{N_1}, and the different behavior of the quantities upon which the closures are based. The complex nonlinear coupling between NLT_{ij}, C_{ij} and S_{ij} (see Appendix A) means that small deviations in the prediction of one quantity will affect the distribution of the other in a complex manner. Nevertheless, in order to obtain a similar DR as in the DNS, what needs to be well predicted are all the shear stresses appearing in the momentum balance and this is reasonably done here. Even though the shear Reynolds stress is underpredicted (Fig. 13) and the polymer shear stress is overpredicted, the sum of these two stresses with the solvent shear stress must be the same as for the DNS to arrive at the same values of Re_{τ_0} and We_{τ_0}. The reasonably good prediction of NLT_{yy} impacts positively the prediction of C_{yy}, as shown in Fig. 16(b)). For the other two components of the conforma-

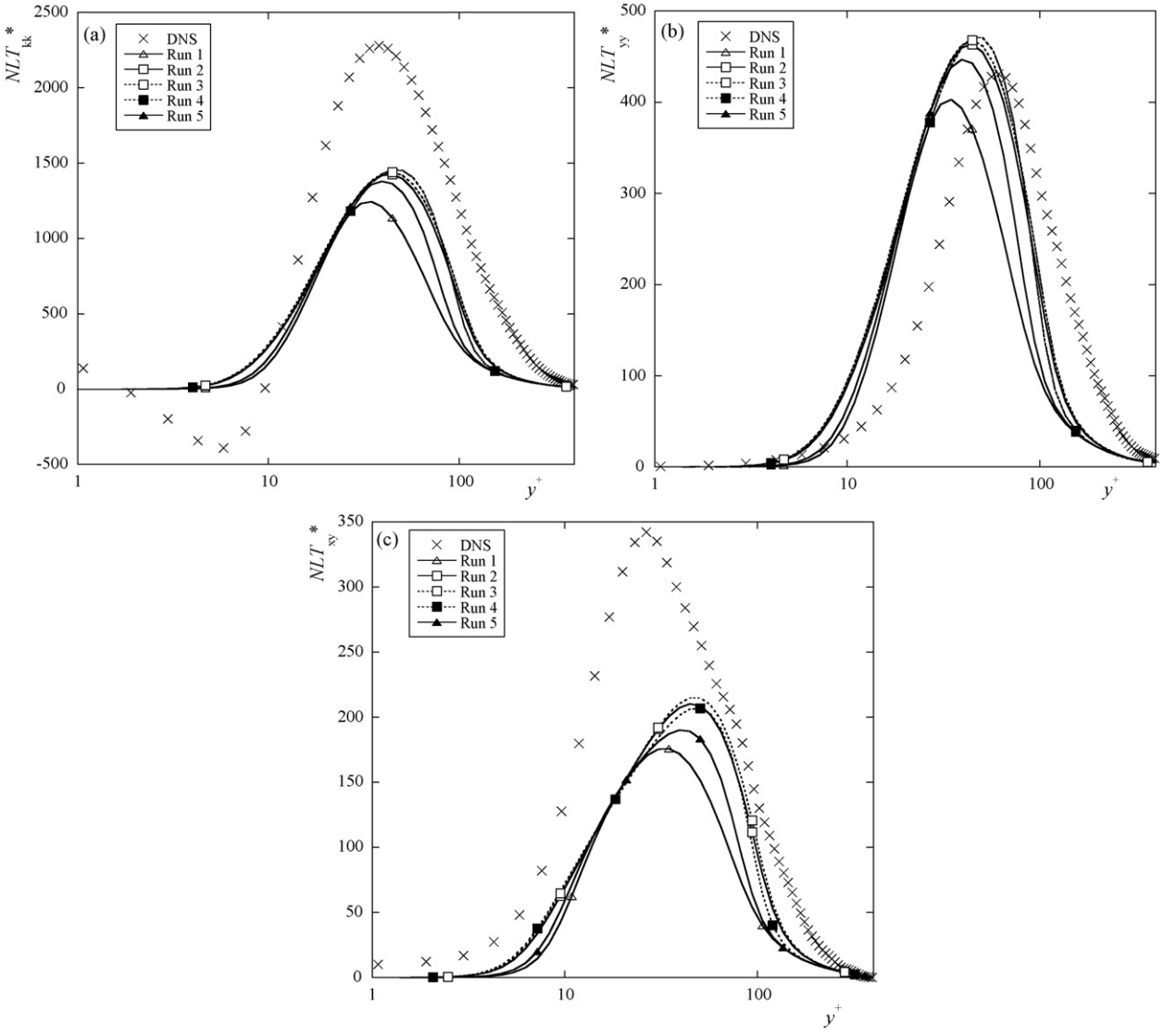

Fig. 15. Comparison between DNS data for FENE-P fluid in turbulent channel flow and the corresponding predictions for runs 1–5 of Table 1. Normalized NLT_{kk} (a), NLT_{yy} (b) and NLT_{xy} (c) as a function of wall distance.

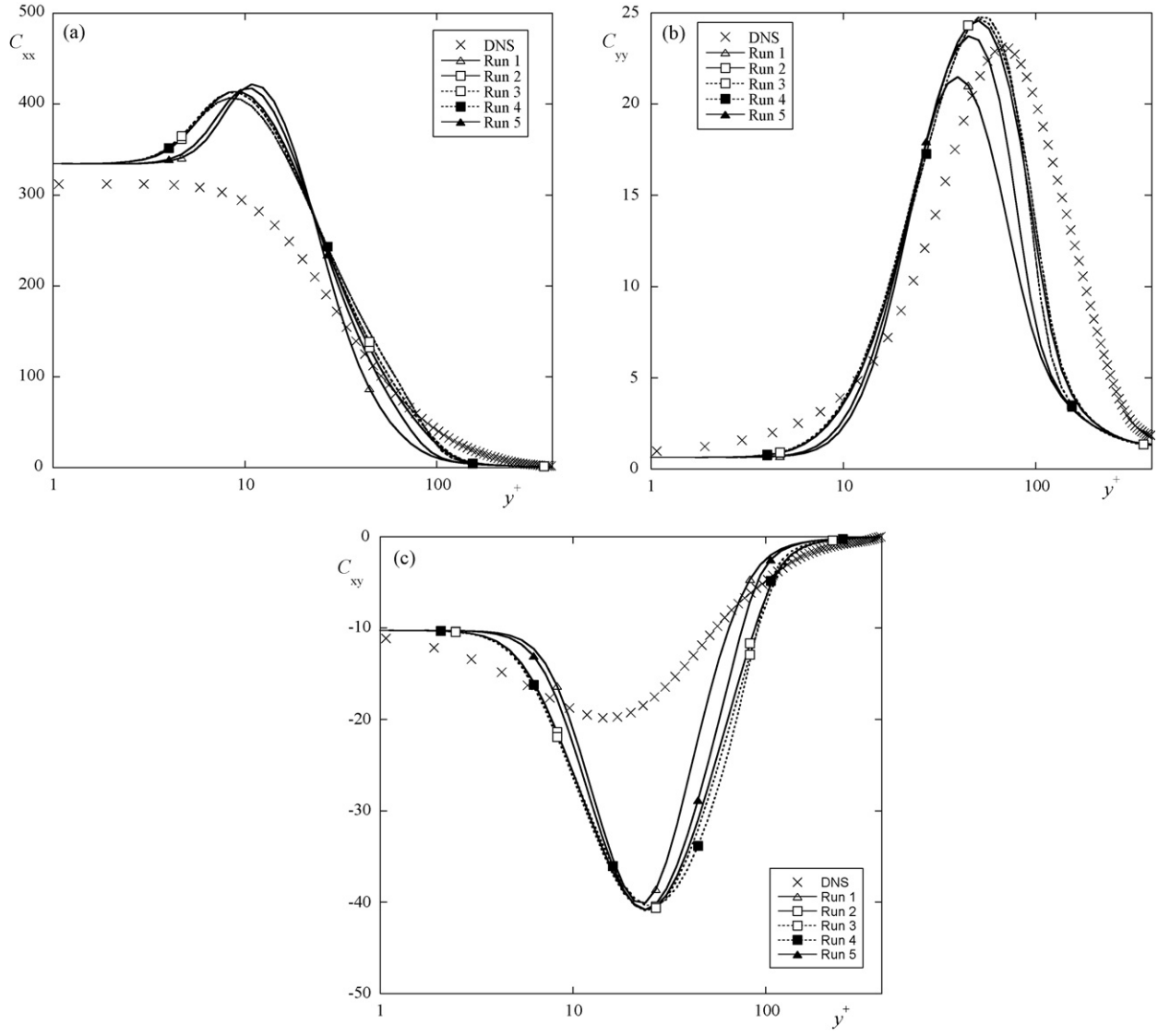

Fig. 16. Comparison between DNS data for FENE-P fluid in turbulent channel flow and the corresponding predictions for runs 1–5 of Table 1. Components of the conformation tensor as a function of wall distance C_{xx} (a), C_{yy} (b) and C_{xy} (c).

tion tensor, C_{xx} is plotted in Fig. 16(a) whereas Fig. 16(c) compares predictions and DNS for C_{xy}. This latter quantity is over-predicted, whereas C_{xx} has an unexpected peak at $y^+ \approx 10$, probably caused by the lack of the small negative peak in NLT_{xx} (and by implication in NLT_{kk}).

5.2. Effects of Weissenberg number, viscosity ratio and molecular extensibility

An appropriate turbulence model would be expected to predict a variable degree of DR as the Weissenberg number is increased. The DNS results show that for We_{τ_0} less than a critical value of around 6 there is no DR, but beyond this value, the degree of DR increases with the Weissenberg number. The performance of the turbulence model of Run 4 in Table 1 was tested as a function of Weissenberg number. The main results are listed in Table 2 and are plotted in Fig. 17. The other models in Table 1 behave similarly. In Fig. 17(a)–(f) profiles are plotted for the normalized mean velocity, turbulent kinetic energy, rate of dissipation of k by the Newtonian solvent, NLT_{ii}, $\bar{\tau}_{\mathrm{p},xy}$ and C_{xx}.

In Fig. 17(a), the predicted profiles of the mean velocity are presented in wall coordinates. For $We_{\tau_0} = 25$, the predictions capture the expected increase in the slope of the log-law whereas the Newtonian results provide a very close match to the universal profile. The results for $We_{\tau_0} \leq 20$ fall below the log-law, which indicates drag enhancement. The remaining comparisons, presented

Table 2
Simulations with model of run 4 (Table 1) at $Re_{\tau_0} = 395$, $L^2 = 900$ and $\beta = 0.9$

We_{τ_0}	Re_τ	We_τ	Re	We	f	DR
Newtonian	395	Newtonian	7047	Newtonian	0.0251	–
0	395	0	6819	0	0.0268	+6.8
5	396.9	5.0	6870	0.22	0.0265	+5.6
10	400.9	10.2	6874	0.44	0.0264	+5.2
15	404.5	15.4	6827	0.66	0.0268	+6.8
20	407.7	20.7	6929	0.89	0.0260	+3.6
22.5	408.9	23.3	7191	1.04	0.0241	−4
25	410.2	26	7856	1.26	0.0202	−19.5

$We_{\tau_0} = \lambda u_\tau^2/\nu_0$, $We_\tau = \lambda u_\tau^2/\nu_w$, $We = \lambda U/h$, $Re_{\tau_0} = hu_\tau/\nu_0$, $Re_\tau = hu_\tau/\nu_w$, $Re = Uh/\nu_0$, ν_w: wall kinematic viscosity, U: bulk velocity, $\mathrm{DR} = (f - f_\mathrm{N})/f_\mathrm{N}$, f_N: Newtonian friction factor.

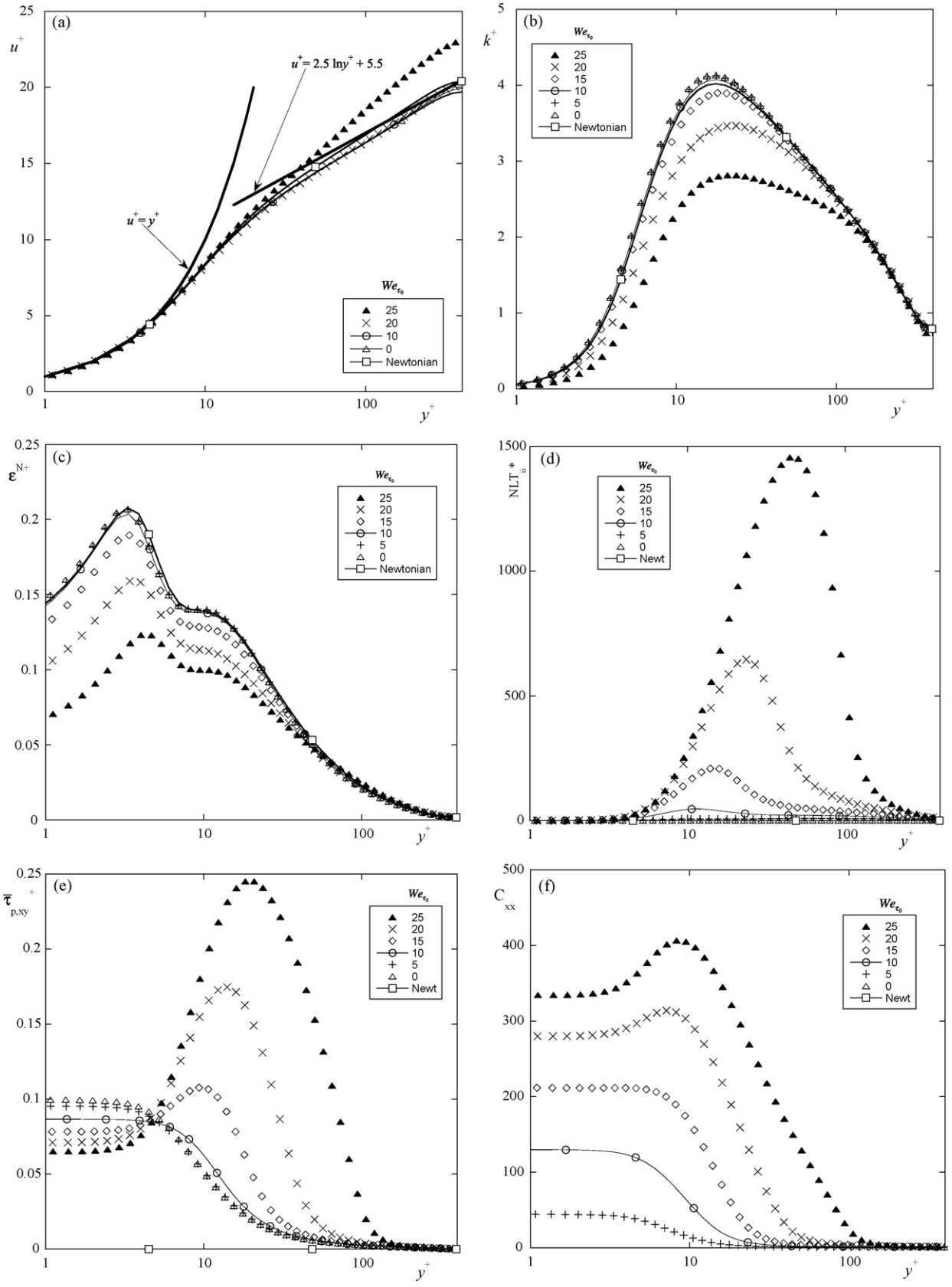

Fig. 17. Effect of Weissenberg number on the channel flow predictions for the turbulence model of run 4 for $Re_{\tau_0} = 395$, $L^2 = 900$ and $\beta = 0.9$. (a) u^+; (b) k^+; (c) ε^{N+}; (d) NLT^*_{ii}; (e) $\bar{\tau}^+_{p,xy}$ and (f) C_{xx}.

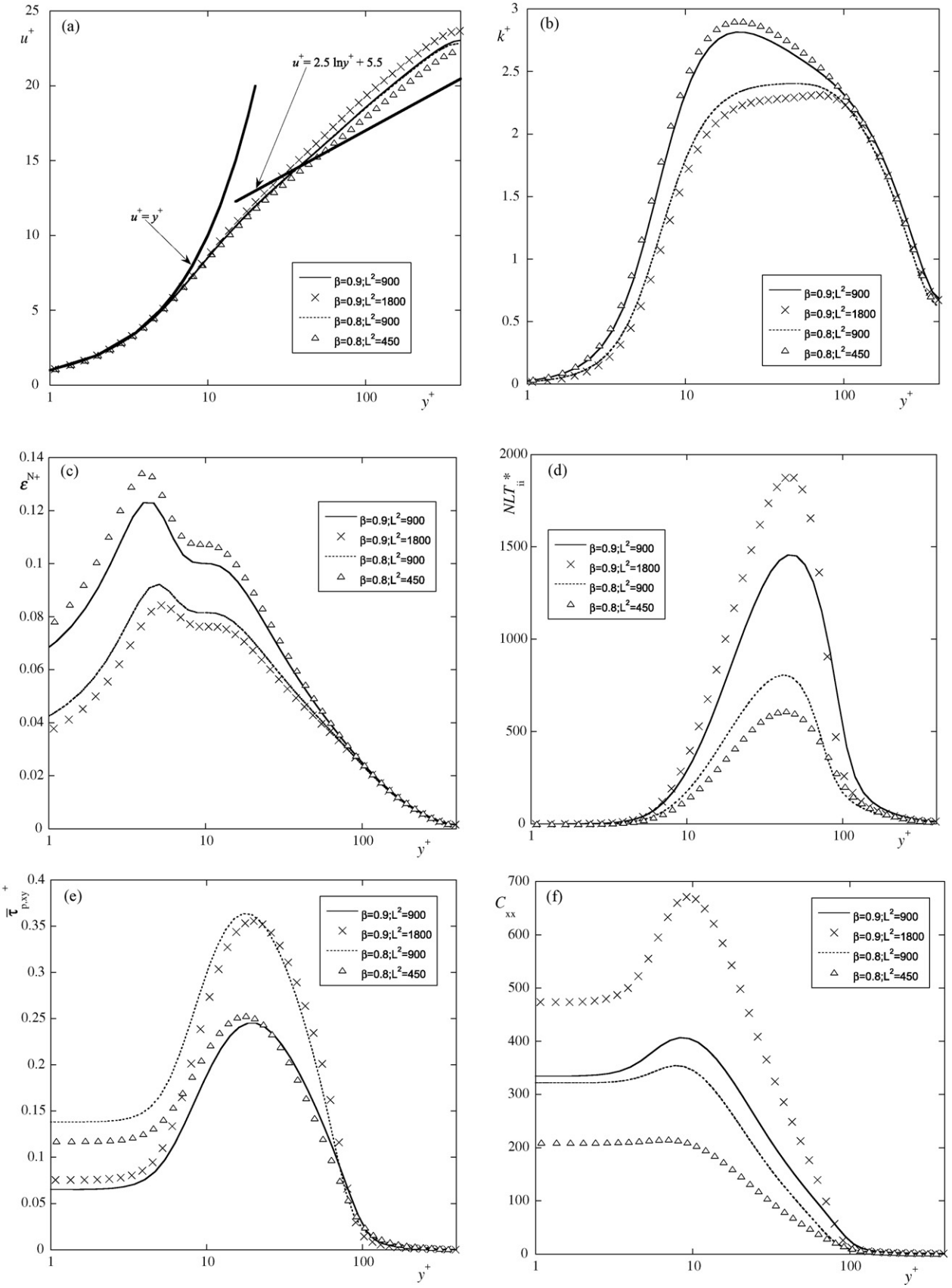

Fig. 18. Effect of L^2 and β on channel flow predictions for the turbulence model of Run 4 for constant bulk velocity, relaxation time and geometry (c.f. Table 3): (a) u^+; (b) k^+; (c) ε^{N+}; (d) NLT^*_{ii}; (e) $\bar{\tau}^+_{p,xy}$; (f) C_{xx}.

in Fig. 17(b)–(f), show a more monotonic dependence of turbulence parameters on the Weissenberg number. The profiles of k (Fig. 17(b)) for $We_{\tau_0} = 0$ and 5 show values that are higher than those of the Newtonian profile. The same is true for ε^{N+} as shown in Fig. 17(c). The other quantities plotted in Fig. 17, $\bar{\tau}_{p,xy}$, C_{xx} and NLT_{ii} show already a monotonic behavior. These results confirm the DNS findings that there is likely no DR at low values of We_{τ_0} and that the onset of this phenomenon starts at a finite critical value of We_{τ_0}. It should be noted that as $We_{\tau_0} \to 0$, the model does not appear to asymptote to its Newtonian limits. That this is the case is because $We_{\tau_0} \to 0$ as a consequence of $\lambda \to 0$. This corresponds to $\eta_p \to 0$ rather than a non-zero value of η_p as in here, since for a FENE-P fluid, λ and η_p are related in the limit of small Weissenberg numbers by $\eta_p \to nk_BT\lambda L^2/(L^2+5)$, where T is the absolute temperature and k_B is Boltzmann's constant [37]. In this specific case the turbulence model will predict correctly the Newtonian flow, but generally the evolution of the predictions with We remains non-monotonic as shown in Fig. 17. Hence, the case $\lambda \to 0$ with $\eta_p \neq 0$ forms a severe test of turbulence model performance. The Newtonian case plotted in Fig. 17 corresponds to $\eta_p = 0$ and a solvent viscosity having the same total viscosity of the polymer solutions, i.e., a viscosity of $\eta_s + \eta_p$, but the results would be identical for a viscosity of η_s at the same Re_{τ_0}.

The behavior at $We_{\tau_0} \to 0$ arises from the closures developed for NLT_{ij} and CU_{ijk}. As $\lambda \to 0$ the closure of NLT_{ij} should result in a purely viscous dissipation associated with the polymer viscosity, whereas the closure for CU_{ijk} should tend to a gradient of the Reynolds stress to give rise to molecular diffusion of the Reynolds stresses by the polymer viscosity. A modified turbulence model that includes corrections to the closures for NLT_{ij} and CU_{ijk} was explored. These corrections deal with the limiting behavior where $\mu_p = \bar{\tau}_{p,xy}/\dot{\gamma}_{xy}$ is the local shear viscosity of the FENE-P fluid and are of the form:

$$f(C_{kk})\,NLT^*_{ij} = \frac{\mu_p}{\eta_p} We_{\tau_0} Re_{\tau_0} \varepsilon^{Np+} + \text{R.H.S. Eq. (25)} \quad \text{and}$$

$$\varepsilon^{Np+} = \frac{\eta_s + \mu_p}{\eta_s} \varepsilon^{N+} \tag{37}$$

$$f(C_{mm})CU^+_{ijk} = \frac{\mu_p}{\eta_p} \frac{We_{\tau_0}}{Re_{\tau_0}} \frac{\partial \overline{u_i u_j}^+}{\partial x^*_k} + \text{R.H.S. Eq. (29)} \tag{38}$$

In the limit of $\lambda \to 0$ the model did indeed produce a monotonic behavior but its performance deteriorated as the Weissenberg number increased as the added corrections overwhelmed the original terms.

To assess the model's sensitivity to L^2 and β, simulations were carried out as listed in Table 3 and plotted in Fig. 18(a)–(f). The model captures the correct response to L^2 in that it predicts a monotonic growth of DR as L^2 increases but this does not seem to be the case with β in the sense that for the same bulk velocity, geometry and relaxation time, reducing β raises the viscosity of the polymer but leaves the pressure drop unchanged. The Reynolds number Re_{τ_0} is reduced, but if this parameter is matched (for instance, by increasing the fluid density) then there is a strong reduction in the friction coefficient, as can be seen in Table 3.

Table 3
Simulations with model and flow conditions of run 4 at $We = 1.26$

L^2	β; $1-\beta$	We_{τ_0}	Re_{τ_0}	We_τ	Re_τ	Re	f
900[a]	0.9; 0.1	25	395	26	410.2	7856	0.0202
1800	0.9; 0.1	23.7	384.6	24.3	395.0	7856	0.0192
900	0.8; 0.2	22.9	356.3	24.6	383.7	6982	0.0208
450	0.8; 0.2	23.8	363.3	26.2	400.6	6982	0.0217
1800	0.9;0.1	23.8	395	24.5	405.7	8249	0.01834
900	0.8;0.2	23.3	395	25.1	425.9	8431	0.01756

[a] Run 4 (from Table 1).

The DNS results for the low DR regime obtained by using different parameters in the FENE-P and Giesekus models suggest that DR is a function of the extensional viscosity of the fluid. For the FENE-P fluid, plateau extensional viscosity is a function of $(1-\beta)L^2$. Hence, the amount of DR obtained using different values of β and L^2 will be similar given that $(1-\beta)L^2$ is held constant. This is not the case here, as shown in the comparison between the two sets of data of Table 3, and of the corresponding curves in Fig. 18. The friction factors in each of these two sets differ by about 10%, suggesting that improvements are required to mimic the relationship between DR and extensional viscosity. For the profiles of k^+ and ε^{N+} there is near collapse of data pertaining to each set, the polymer stresses are not too different, but for NLT_{ii} there are significant differences. Since NLT_{ii} affects ε^V, which is used to calculate the eddy viscosity in the model of run 4, this should be the cause for the 10% difference seen in the friction factor.

6. Closure

A framework for turbulence closures of the Reynolds-average Navier–Stokes equations for viscoelastic fluids represented by the FENE-P rheological constitutive model has been developed leading to a self-consistent system of model equations. DNS results were analyzed to identify dominant terms from the perspective of the development of single-point two-equation closures. The methodology advanced here is extensible to the more reliable second-order closures for the Reynolds stresses. The outcome of this work is a proposal for a robust yet accurate $k-\varepsilon$ model, which was incorporated into a finite-volume computational method and used to predict fully developed channel flows of FENE-P fluids. This model is of the low turbulence Reynolds number variety and is modified to account for variable turbulent diffusion coefficients in the k and ε equations. A central feature of this model is the inclusion of two viscoelastic terms in the transport equations of turbulent kinetic energy: the viscoelastic stress work and the viscoelastic turbulent transport term. The model requires the solution of the conformation tensor evolution equation, which contains the new turbulent distortion term (NLT_{ij}), the correlation between the fluctuating conformation (c_{ij}) and rate of strain ($\partial u_i/\partial x_j$) tensors.

Analysis of the DNS results showed that the viscoelastic stress work is adequately modeled by the trace of NLT_{ij} and simple closures for NLT_{ij} whereas the viscoelastic turbulent transport terms were formulated using *a priori* DNS analysis. The model, despite its ability to reproduce many of the flow features obtained in the DNS results, does not succeed in capturing the region of negative NLT_{xx} close to the wall. This, and other shortcomings, may be resolved by adoption of a better Newtonian model. This will also improve the model's performance in the limit of vanishing relaxation times where a Newtonian behavior needs to be obtained.

Acknowledgements

This work was initiated during FT Pinho's stay at the Department of Civil and Environmental Engineering at the University of California, Davis and at the Department of Chemical Engineering at Washington University of St. Louis during his 2005–2006 sabbatical leave. FTP thanks Fundação Calouste Gulbenkian (Scholarship 72259) and Fundação para a Ciência e a Tecnologia (Scholarship SFRH/BSAB/507/2005) for funding these extended stays, and gratefully acknowledges further funding from FEDER and FCT via project POCI/56342/EQU/2004. R.S. would like to acknowledge NSF CTS grant 0335348. During these extended periods in the US, FTP acknowledges the many discussions with colleagues, especially

Prof. Bamin Khomami, now of the University of Tennessee in Knoxville.

Appendix A. Polymer stress, shear viscosity and conformation tensor for a FENE-P fluid in fully developed turbulent channel flow

The polymer shear stress in fully developed turbulent channel flow according to the simplifications introduced in Section 3 is

$$\bar{\tau}_{xy,\mathrm{p}} = \frac{\eta_\mathrm{p}}{\lambda} f(C_{kk}) C_{xy} \tag{AI.1}$$

The components C_{xx}, C_{xy}, C_{yy} and C_{zz} of the conformation tensor must be calculated by the general Eq. (31) which for this flow are given by the following equations:

$$2\lambda C_{xy}\frac{\mathrm{d}U}{\mathrm{d}y} + \lambda\,\mathrm{NLT}_{xx} = f(C_{kk})C_{xx} - f(L) \tag{AI.2-a}$$

$$\lambda C_{yy}\frac{\mathrm{d}U}{\mathrm{d}y} + \lambda\,\mathrm{NLT}_{xy} = f(C_{kk})C_{xy} \tag{AI.2-b}$$

$$\lambda\,\mathrm{NLT}_{yy} = f(C_{kk})C_{yy} - f(L) \tag{AI.2-c}$$

$$\lambda\,\mathrm{NLT}_{zz} = f(C_{kk})C_{zz} - f(L) \tag{AI.2-d}$$

$$\lambda C_{zy}\frac{\mathrm{d}U}{\mathrm{d}y} + \lambda\,\mathrm{NLT}_{zx} = f(C_{kk})C_{zx} \tag{AI.2-e}$$

$$\lambda\,\mathrm{NLT}_{zy} = f(C_{kk})C_{zy} \tag{AI.2-f}$$

$C_{xz} = C_{yz} = 0$ are solutions of Eqs. (AI.2-e) and (AI.2-f). By back-substitution, the other components of C_{ij} are made to depend on a single component of the conformation tensor. Here, the following set of equations is used:

$$C_{xx} = L^2 - C_{yy}\frac{L^2 - 1 + \lambda(\mathrm{NLT}_{yy} + \mathrm{NLT}_{zz})}{\lambda\,\mathrm{NLT}_{yy} + 1} \tag{AI.3-a}$$

$$C_{zz} = C_{yy}\frac{\lambda\,\mathrm{NLT}_{zz} + 1}{\lambda\,\mathrm{NLT}_{yy} + 1} \tag{AI.3-b}$$

$$C_{xy} = C_{yy}\frac{\lambda\,\mathrm{NLT}_{xy} + \lambda C_{yy}(\mathrm{d}U/\mathrm{d}y)}{\lambda\,\mathrm{NLT}_{yy} + 1} \tag{AI.3-c}$$

By back-substitution, the following cubic equation on C_{yy} is obtained:

$$C_{yy}^3 + a_1 C_{yy}^2 + a_2 C_{yy} + a_3 = 0 \tag{AI-4}$$

with coefficients

$$a_1 = \frac{\mathrm{NLT}_{xy}}{\mathrm{d}U/\mathrm{d}y};$$

$$a_2 = \frac{[L^2 - \lambda(\mathrm{NLT}_{xx} + \mathrm{NLT}_{yy} + \mathrm{NLT}_{zz})](\lambda\,\mathrm{NLT}_{yy} + 1)}{2(\lambda(\mathrm{d}U/\mathrm{d}y))^2};$$

$$a_3 = -\frac{L^2(\lambda\,\mathrm{NLT}_{yy} + 1)^2}{2\left(\lambda(\mathrm{d}U/\mathrm{d}y)\right)^2} \tag{AI-5}$$

Defining the parameters

$$a = a_2 - \frac{a_1^2}{3}; \qquad b = a_3 - \frac{a_1 a_2}{3} + \frac{2a_1^3}{27};$$

$$d = \frac{b^2}{4} + \frac{a^3}{27}; \qquad r = \sqrt{\frac{-a^3}{27}} \quad \text{and} \quad \omega = \arccos\left(\frac{-b}{2r}\right) \tag{AI-6}$$

the three solutions of this cubic equation are

(1) If $d > 0$ there are two complex solutions and one real solution, the latter given by

$$C_{yy} = p^{1/3} + q^{1/3} - \frac{a_1}{3} \quad \text{where} \quad p = -\frac{b}{2} + \sqrt{d} \quad \text{and}$$

$$q = -\frac{b}{2} - \sqrt{d} \tag{AI-7}$$

(2) If $d < 0$ there are three real solutions

$$C_{yy} = 2\sqrt{\frac{-a}{3}}\cos\left(\frac{\omega}{3}\right) - \frac{a_1}{3} \tag{AI.8-a}$$

$$C_{yy} = 2\sqrt{\frac{-a}{3}}\cos\left(\frac{\omega + 2\pi}{3}\right) - \frac{a_1}{3} \tag{AI.8-b}$$

$$C_{yy} = 2\sqrt{\frac{-a}{3}}\cos\left(\frac{\omega + 4\pi}{3}\right) - \frac{a_1}{3} \tag{AI.8-c}$$

To determine the correct solution, the behavior of the FENE-P model must be analyzed and realizability of C_{ij} imposed. For this constitutive equation the trace of the conformation tensor must always be within 3 and L^2, corresponding to a dumbbell in the equilibrium state and fully extended, respectively.

Appendix B. Transport equation for the Reynolds stresses

The transport equation for the Reynolds stress of a FENE-P fluid is [42]:

$$\rho\frac{\partial\overline{u_i u_j}}{\partial t} + \rho U_k\frac{\partial\overline{u_i u_j}}{\partial x_k} = P_{ij} + Q_{ij} + Q_{ij}^\mathrm{V} + D_{ij,\mathrm{N}} + \Pi_{ij} - \rho\varepsilon_{ij}^\mathrm{N} - \rho\varepsilon_{ij}^\mathrm{V}, \tag{AII-1}$$

where $P_{ij} = -\rho\left(\overline{u_i u_k}(\partial U_j/\partial x_k) + \overline{u_j u_k}(\partial U_i/\partial x_k)\right)$, the rate of production of Reynolds stresses; $Q_{ij} = -(\partial/\partial x_k)(\rho\overline{u_i u_j u_k})$, the turbulent transport of Reynolds stress; $D_{ij}^\mathrm{N} = \eta_\mathrm{s}(\partial^2\overline{u_i u_j}/\partial x_k\partial x_k)$, the molecular diffusion associated with the Newtonian solvent; $\Pi_{ij} = -\left(\overline{u_i(\partial p'/\partial x_j)} + \overline{u_j(\partial p'/\partial x_i)}\right)$, the pressure correlations, encompassing both the redistributive pressure strain term, $\overline{p'(\partial u_i/\partial x_j)} + \overline{p'(\partial u_j/\partial x_i)}$, and the term associated with turbulent transport, $-(\partial\overline{p'u_i}/\partial x_j) - (\partial\overline{p'u_j}/\partial x_i)$; $\varepsilon_{ij}^\mathrm{N} = 2\nu_\mathrm{s}\overline{(\partial u_i/\partial x_k)(\partial u_j/\partial x_k)}$, the direct viscous dissipation due to the Newtonian solvent (superscript N). For convenience and by analogy with turbulence for Newtonian fluids, we define the viscous dissipation with the solvent kinematic viscosity and we use the opposite sign to that of the original work [42].

The two new terms in Eq. (AII-1) are $Q_{ij}^\mathrm{V} = \frac{\partial}{\partial x_k}(\overline{u_i\tau'_{jk,\mathrm{p}}} + \overline{u_j\tau'_{ik,\mathrm{p}}})$, the viscoelastic turbulent transport due to fluctuating viscoelastic stresses; $\varepsilon_{ij}^\mathrm{V} = \frac{1}{\rho}\left(\overline{\tau'_{jk,\mathrm{p}}\frac{\partial u_i}{\partial x_k}} + \overline{\tau'_{ik,\mathrm{p}}\frac{\partial u_j}{\partial x_k}}\right)$, the stress power, representing energy per unit time that the chains can dissipate or store as free energy, it quantifies the work done by the viscoelastic stresses. This is sometimes referred to as viscoelastic dissipation [42,43] given the similarity to the viscous dissipation $\varepsilon_{ij}^\mathrm{N}$, but the concept of power is more appropriate since it can have positive and negative contributions in contrast with a dissipative term.

The definition of the polymeric stress of Eq. (5) can be used to expand the two new viscoelastic terms, which become:

$$Q_{ij}^\mathrm{V} = \frac{\eta_\mathrm{p}}{\lambda}\frac{\partial}{\partial x_k}[C_{ik}\overline{f(C_{mm} + c_{mm})u_j} + C_{jk}\overline{f(C_{mm} + c_{mm})u_i} + \overline{f(C_{mm} + c_{mm})c_{ik}u_j} + \overline{f(C_{mm} + c_{mm})c_{jk}u_i}] \tag{AII-2}$$

$$\varepsilon_{ij}^{V} = \frac{\eta_p}{\rho\lambda}\left[C_{ik}\overline{f(C_{mm}+c_{mm})\frac{\partial u_j}{\partial x_k}} + C_{jk}\overline{f(C_{mm}+c_{mm})\frac{\partial u_i}{\partial x_k}} + \overline{f(C_{mm}+c_{mm})c_{ik}\frac{\partial u_j}{\partial x_k}} + \overline{f(C_{mm}+c_{mm})c_{jk}\frac{\partial u_i}{\partial x_k}}\right] \quad \text{(AII-3)}$$

Appendix C. Transport equation for the rate of dissipation of turbulent kinetic energy by the Newtonian solvent for a FENE-P fluid

To obtain the transport equation for the rate of dissipation of k by the solvent for a FENE-P fluid we follow [58,28] to obtain:

$$2\eta_s\overline{\frac{\partial u_i}{\partial x_m}\frac{\partial}{\partial x_m}(Lu_i)} = 0, \quad \text{(AIII-1)}$$

where Lu_i is the equation of the fluctuations of the i-velocity component (Eq. (AIII-2))

$$Lu_i : \rho\frac{\partial u_i}{\partial t} + \rho U_k\frac{\partial u_i}{\partial x_k} + \rho u_k\frac{\partial U_i}{\partial x_k} + \rho\frac{\partial}{\partial x_k}(u_iu_k - \overline{u_iu_k}) = -\frac{\partial p'}{\partial x_i} + \frac{\partial}{\partial x_k}(2\eta_s s_{ik} + \tau'_{ik,p}) \quad \text{(AIII-2)}$$

The tensor s_{ik} is the fluctuating rate of deformation and the fluctuating polymer stress (τ'^{p}_{ik}) and is given by

$$\tau'_{ik,p} \equiv \hat{\tau}_{ik,p} - \bar{\tau}_{ik,p} = \frac{\eta_p}{\lambda}\{[f(\hat{C}_{nn}) - f(C_{nn})]C_{ik} - \overline{f(\hat{C}_{nn})c'_{ik}}\} \quad \text{(AIII-3)}$$

Using Eq. (6) it can be shown that $f(\hat{C}_{nn}) - f(C_{nn}) = f(C_{nn})f(\hat{C}_{pp})(c'_{qq}/(L^2-3))$.

Performing the operations in Eq. (AIII-1) leads to

$$\underbrace{2\nu_s\overline{\frac{\partial u_i}{\partial x_m}\frac{\partial}{\partial x_m}\left(\rho\frac{Du_i}{Dt}\right)}}_{\text{I and II}} + \underbrace{2\nu_s\overline{\frac{\partial u_i}{\partial x_m}\frac{\partial}{\partial x_m}\left(\rho u_k\frac{\partial U_i}{\partial x_k}\right)}}_{\text{III}} + \underbrace{2\nu_s\overline{\frac{\partial u_i}{\partial x_m}\frac{\partial}{\partial x_m}\left(\rho\frac{\partial u_iu_k}{\partial x_k}\right)}}_{\text{IV}} + \underbrace{2\nu_s\overline{\frac{\partial u_i}{\partial x_m}\frac{\partial}{\partial x_m}\left(\frac{\partial p'}{\partial x_i}\right)}}_{\text{V}} - \underbrace{4\rho\nu_s^2\overline{\frac{\partial u_i}{\partial x_m}\frac{\partial}{\partial x_m}\left(\frac{\partial s_{ik}}{\partial x_k}\right)}}_{\text{VI}} - \underbrace{2\nu_s\overline{\frac{\partial u_i}{\partial x_m}\frac{\partial}{\partial x_m}\left(\frac{\partial \tau'_{ik,p}}{\partial x_k}\right)}}_{\text{VII}} = 0 \quad \text{(AIII-4)}$$

Introducing the following definitions of average and fluctuating rates of dissipation

$$\varepsilon^N \equiv \nu_s\overline{\frac{\partial u_i}{\partial x_m}\frac{\partial u_i}{\partial x_m}} \quad \text{and} \quad \varepsilon^{N'} \equiv \nu_s\frac{\partial u_i}{\partial x_m}\frac{\partial u_i}{\partial x_m} \quad \text{(AIII-5)}$$

the terms of Eq. (AIII-4) become:

Terms I and II

$$2\nu_s\overline{\frac{\partial u_i}{\partial x_m}\frac{\partial}{\partial x_m}\left(\rho\frac{Du_i}{Dt}\right)} = 2\nu_s\overline{\frac{\partial u_i}{\partial x_m}\frac{\partial}{\partial x_m}\left(\rho\frac{\partial u_i}{\partial t}\right)} + 2\nu_s\overline{\frac{\partial u_i}{\partial x_m}\frac{\partial}{\partial x_m}\left(\rho U_k\frac{\partial u_i}{\partial x_k}\right)} = \rho\frac{\partial\varepsilon^N}{\partial t} + \rho U_k\frac{\partial\varepsilon^N}{\partial x_k} + 2\eta_s\frac{\partial U_k}{\partial x_m}\overline{\frac{\partial u_i}{\partial x_m}\frac{\partial u_i}{\partial x_k}} \quad \text{(AIII-6)}$$

Term III

$$2\nu_s\overline{\frac{\partial u_i}{\partial x_m}\frac{\partial}{\partial x_m}\left(\rho u_k\frac{\partial U_i}{\partial x_k}\right)} = 2\eta_s\frac{\partial U_i}{\partial x_k}\overline{\frac{\partial u_i}{\partial x_m}\frac{\partial u_k}{\partial x_m}} + 2\eta_s\frac{\partial^2 U_i}{\partial x_m\partial x_k}\overline{u_k\frac{\partial u_i}{\partial x_m}} \quad \text{(AIII-7)}$$

Term IV

$$2\nu_s\overline{\frac{\partial u_i}{\partial x_m}\frac{\partial}{\partial x_m}\left(\rho\frac{\partial u_iu_k}{\partial x_k}\right)} = 2\eta_s\overline{\frac{\partial u_i}{\partial x_k}\frac{\partial u_i}{\partial x_m}\frac{\partial u_k}{\partial x_m}} + \rho\frac{\partial}{\partial x_k}(\overline{u_k\varepsilon^{N'}}) \quad \text{(AIII-8)}$$

Term V

$$2\nu_s\overline{\frac{\partial u_i}{\partial x_m}\frac{\partial}{\partial x_m}\left(\frac{\partial p'}{\partial x_i}\right)} = 2\nu_s\frac{\partial}{\partial x_i}\left(\overline{\frac{\partial p'}{\partial x_m}\frac{\partial u_i}{\partial x_m}}\right) \quad \text{(AIII-9)}$$

Term VI

$$-4\rho\nu_s^2\overline{\frac{\partial u_i}{\partial x_m}\frac{\partial}{\partial x_m}\left(\frac{\partial s_{ik}}{\partial x_k}\right)} = -\eta_s\frac{\partial^2\varepsilon^N}{\partial x_k\partial x_k} + 2\eta_s\nu_s\overline{\frac{\partial^2 u_i}{\partial x_k\partial x_m}\frac{\partial^2 u_i}{\partial x_k\partial x_m}} \quad \text{(AIII-10)}$$

Term VII

$$-2\nu_s\overline{\frac{\partial u_i}{\partial x_m}\frac{\partial}{\partial x_m}\left(\frac{\partial\tau'_{ik,p}}{\partial x_k}\right)} = -2\nu_s\frac{\eta_p}{\lambda(L^2-3)}\overline{\frac{\partial u_i}{\partial x_m}\frac{\partial}{\partial x_m}\left\{\frac{\partial}{\partial x_k}[f(C_{nn})f(\hat{C}_{pp})c'_{qq}C_{ik}]\right\}} \quad \text{(AIII-11)}$$

Grouping all terms together, the final form of the equation is

$$\rho\frac{\partial\varepsilon^N}{\partial t} + \rho U_k\frac{\partial\varepsilon^N}{\partial x_k} = -2\eta_s\left[\overline{\frac{\partial U_i}{\partial x_m}\frac{\partial u_i}{\partial x_m}\frac{\partial u_i}{\partial x_k}} + \overline{\frac{\partial U_i}{\partial x_k}\frac{\partial u_i}{\partial x_m}\frac{\partial u_k}{\partial x_m}}\right] - 2\eta_s\frac{\partial^2 U_i}{\partial x_m\partial x_k}\overline{u_k\frac{\partial u_i}{\partial x_m}} - 2\eta_s\overline{\frac{\partial u_i}{\partial x_m}\frac{\partial u_i}{\partial x_k}\frac{\partial u_k}{\partial x_m}} - \frac{\partial}{\partial x_k}\left[\rho\overline{u_k\varepsilon^{N'}} + 2\nu_s\overline{\frac{\partial p'}{\partial x_m}\frac{\partial u_k}{\partial x_m}}\right] + \eta_s\frac{\partial^2\varepsilon^N}{\partial x_k\partial x_k} - 2\eta_s\nu_s\overline{\frac{\partial^2 u_i}{\partial x_m\partial x_k}\frac{\partial^2 u_i}{\partial x_m\partial x_k}} + 2\nu_s\frac{\eta_p}{\lambda(L^2-3)} \times \overline{\frac{\partial u_i}{\partial x_m}\frac{\partial}{\partial x_m}\left\{\frac{\partial}{\partial x_m}[f(C_{nn})f(\hat{C}_{pp})c'_{qq}C_{ik}]\right\}} \quad \text{(AIII-12)}$$

References

[1] G.K. Patterson, J. Chosnek, J.L. Zakin, Turbulence structure in drag-reducing polymer solutions, Phys. Fluids 20 (1977) S89–S99.
[2] A. Gyr, H.-W. Bewersdorff, Drag Reduction by Additives. Fluid Mechanics and its Aplications Series, vol. 32, Kluwer Academic Publishers, Dordrecht, 1995.
[3] J.W. Hoyt, Drag reduction effectiveness of polymer solutions in the turbulent flow rheometer: a catalog, Polym. Lett. 9 (1971) 851–862.
[4] N.S. Berman, Drag reduction of the highest molecular weight fractions of polyethylene oxide, Phys. Fluids 20 (1977) 715–718.
[5] J.W. Hoyt, The effect of additives on fluid friction, ASME J. Basic Eng. 94 (1972) 258–285.
[6] P.S. Virk, Drag reduction fundamentals, AIChE J. 21 (1975) 625–656.
[7] F.A. Seyer, A.B. Metzner, Turbulence phenomena in drag reducing systems, AIChE J. 15 (1969) 426–434.
[8] J.L. Lumley, Drag reduction by additives, Ann. Rev. Fluid Mech. 1 (1969) 367–386.
[9] E.J. Hinch, Mechanical models of dilute polymer solutions in strong flows, Phys. Fluids 20 (1977) S22–S30.
[10] G. Ryskin, Turbulent drag reduction by polymers: a quantitative theory, Phys. Rev. Lett. 59 (1987) 2059–2062.
[11] M. Tabor, P.G. De Gennes, A cascade theory of drag reduction, Europhys. Lett. 2 (1986) 519–522.
[12] H. Massah, T.J. Hanratty, Added stresses because of the presence of FENE-P bead-spring chains in a random velocity field, J. Fluid Mech. 337 (1997) 67–101.
[13] T. Min, J.Y. Yoo, H. Choi, D.D. Joseph, Drag reduction by polymer additives in a turbulent channel flow, J. Fluid Mech. 486 (2003) 213–238.
[14] R. Sureshkumar, A.N. Beris, R.A. Handler, Direct numerical simulation of the turbulent channel flow of a polymer solution, Phys. Fluids 9 (1997) 743–755.
[15] P.K. Ptasinski, B.J. Boersma, F.T.M. Nieuwstadt, M.A. Hulsen, B.H.A.H. van den Brule, J.C.R. Hunt, Turbulent channel flow near maximum drag reduction: simulations, experiments and mechanisms, J. Fluid Mech. 490 (2003) 251–291.

[16] E. De Angelis, C.M. Casciola, R. Piva, DNS of wall turbulence: dilute polymers and self-sustaining mechanisms, Comput. Fluids 31 (2002) 495–507.
[17] R.B. Bird, P.J. Dotson, N.L. Johnson, Polymer solution rheology based on a finitely extensible bead-spring chain model, J. Non-Newton. Fluid Mech. 7 (1980) 213–235.
[18] C.D. Dimitropoulos, R. Sureshkumar, A.N. Beris, Direct numerical simulation of viscoelastic turbulent channel flow exhibiting drag reduction: the effect of variation of rheological parameters, J. Non-Newton. Fluid Mech. 79 (1998) 433–468.
[19] C.D. Dimitropoulos, Y. Dubief, E.S.G. Shaqfeh, P. Moin, S.K. Lele, Direct numerical simulation of polymer-induced drag reduction in turbulent boundary layer flow, Phys. Fluids 17 (2005) (paper 011705).
[20] K. Kim, C.F. Li, R. Sureshkumar, S. Balachandar, R. Adrian, Effects of polymer stresses on eddy structures in drag-reduced turbulent channel flow, J. Fluid Mech. 584 (2007) 281–299.
[21] K. Kim, R.J. Adrian, S. Balachandar, R. Sureshkumar, Dynamics of hairpin vortices and polymer-induced turbulent drag reduction, Phys. Rev. Lett., in press.
[22] P.A. Stone, A. Roy, R.G. Larson, F. Waleffe, M.D. Graham, Polymer drag reduction in exact coherent structures of plane shear flow, Phys. Fluids 16 (9) (2004) 3470–3482.
[23] W. Li, X. Li, M.D. Graham, Non-linear travelling waves as a framework for understanding turbulent drag reduction, J. Fluid Mech. 565 (2006) 353–362.
[24] C.-F. Li, R. Sureshkumar, B. Khomami, Influence of molecular parameters on polymer induced turbulent drag reduction, J. Non-Newton. Fluid Mech. 140 (2006) 23–40.
[25] F. Durst, A.K. Rastogi, Calculations of turbulent boundary layer flows with drag reducing polymer additives, Phys. Fluids 20 (1977) 1975–1985.
[26] S. Hassid, M. Poreh, A turbulent energy dissipation model for flows with drag reduction, ASME J. Fluids Eng. 100 (1978) 107–112.
[27] T. Mizushina, H. Usui, Reduction of eddy diffusion for momentum and heat in viscoelastic fluid flow in a circular tube, Phys. Fluids 20 (1977) S100–S107.
[28] F.T. Pinho, A GNF framework for turbulent flow models of drag reducing fluids and proposal for a $k-\varepsilon$ type closure, J. Non-Newton. Fluid Mech. 114 (2003) 149–184.
[29] F.T. Pinho, B. Sadanandan, R. Sureshkumar, One equation model for turbulent channel flow with second order viscoelastic corrections, Flow Turbul. Combust., doi:10.1007/s10494-008-9134-6.
[30] M.R. Malin, Turbulent pipe flow of power law fluids, Int. Commun. Heat Mass Transf. 24 (1997) 977–988.
[31] M.R. Malin, Turbulent pipe flow of Herschel–Bulkley fluids, Int. Commun. Heat Mass Transf. 25 (1998) 321–330.
[32] D.O.A. Cruz, C.E. Maneschy, E.N. Macedo, J.N.N. Quaresma, A turbulence model for computing the flow of power law fluids within circular tubes, Hybrid Methods Eng. 2 (2000) 1–13.
[33] D.O.A. Cruz, F.T. Pinho, Turbulent flow predictions with a low Reynolds number $k-\varepsilon$ model for drag reducing fluids, J. Non-Newton. Fluid Mech. 114 (2003) 109.
[34] D.O.A. Cruz, F.T. Pinho, P.R. Resende, Modeling the new stress for improved drag reduction predictions of viscoelastic pipe flow, J. Non-Newton. Fluid Mech. 121 (2004) 127.
[35] P.R. Resende, M.P. Escudier, F. Presti, F.T. Pinho, D.O.A. Cruz, Numerical predictions and measurements of Reynolds normal stresses in turbulent pipe flow of polymers, Int. J. Heat Fluid Flow 27 (2006) 204.
[36] P.R. Resende, F.T. Pinho, D.O.A. Cruz, A Reynolds stress model for turbulent pipe flow of viscoelastic fluids, in: Proceedings of the First National Conference on Numerical Methods for Fluid Mechanics and Thermodynamics (1ª Conferência Nacional de de Métodos Numéricos em Mecânica dos Fluidos e Termodinâmica), Portugal, June 8–9, 2006 (CD-ROM, paper Art06.pdf, Costa da Caparica).
[37] R.B. Bird, C.F. Curtiss, R.C. Armstrong, O. Hassager, Dynamics of polymeric liquids Kinetic Theory, vol. 2, 2nd ed., John Wiley & Sons, New York, 1987.
[38] C.-F. Li, V.K. Gupta, R. Sureshkumar, B. Khomami, Turbulent channel flow of dilute polymeric solutions: drag reduction scaling and an eddy viscosity model, J. Non-Newton. Fluid Mech. 139 (2006) 177–189.
[39] S.B. Pope, Turbulent Flows, Cambridge University Press, Cambridge, UK, 2000.
[40] Y. Nagano, M. Hishida, Improved form of the $k-\varepsilon$ model for wall turbulent shear flows, ASME J. Fluids Eng. 109 (1987) 156–160.
[41] T.S. Park, H.J. Sung, A nonlinear low-Reynolds-number $k-\varepsilon$ model for turbulent separated and reattaching flows. I. Flow field computations, Int. J. Heat Mass Transf. 38 (1995) 2657–2666.
[42] C.D. Dimitropoulos, R. Sureshkumar, A.N. Beris, R.A. Handler, Budgets of Reynolds stress, kinetic energy and streamwise enstrophy in viscoelastic turbulent channel flow, Phys. Fluids 13 (4) (2001) 1016–1027.
[43] K.D. Housiadas, A.N. Beris, R.A. Handler, Viscoelastic effects on higher order statistics and coherent structures in turbulent channel flow, Phys. Fluids 17 (2005) (paper 35106).
[44] A.N. Beris, B.J. Edwards, Thermodynamics of Flowing Systems with Internal Microstructure, Oxford University Press, New York, 1994.
[45] W.P. Jones, B.E. Launder, The prediction of laminarization with a two-equation model of turbulence, Int. J. Heat Mass Transf. 15 (1972) 301–314.
[46] Y. Nagano, M. Shimada, Modeling the dissipation-rate equation for two-equation turbulence model, in: Ninth Symposium on Turbulent Shear Flows, Kyoto, Japan, August 16–18, 1993 (paper 23–2).
[47] M.M. Rahman, T. Siikonen, Low Reynolds number $k-\varepsilon$ model for near-wall flow, Int. J. Num. Methods Fluids 47 (2005) 325–338.
[48] K. Hanjalic, Advanced turbulence closure models: a view of current status and future prospects, Int. J. Heat Fluid Flow 15 (1994) 178–203.
[49] N.N. Mansour, J. Kim, P. Moin, Reynolds stress and dissipation rate budgets in a turbulent channel flow, J. Fluid Mech. 194 (1988) 15–44.
[50] W. Rodi, On the equation governing the rate of turbulent energy dissipation, Internal Report, Imperial College, Mech. Eng. Dept., University of London, UK, Rept. TM/TN/A/14, 1971.
[51] K. Hanjalic, B.E. Launder, A Reynolds stress model of turbulence and its application to thin shear flows, J. Fluid Mech. 52 (1972) 609–632.
[52] A.P. Morse, Axisymmetric free shear flows with and without swirl, Ph.D. Thesis, University of London, London, UK, 1980.
[53] F.T. Pinho, Time-average double-correlations in turbulence models of FENE-P viscoelastic fluids, Internal report of Centro de Estudos de Fenómenos de Transporte (CEFT), Faculdade de Engenharia da Universidade do Porto, Portugal, November 22, 2005.
[54] B.A. Younis, C.G. Speziale, T.T. Clark, A rational model for the turbulent scalar fluxes, Proc. R. Soc. A 461 (2005) 575–594.
[55] B.A. Younis, T.B. Gatski, C.G. Speziale, Towards a rational model for the triple velocity correlations of turbulence, Proc. R. Soc. A 456 (2000) 909–920.
[56] B.A. Younis, A computer programme for two-dimensional turbulent boundary layer flow, Internal report, Department of Civil Engineering, City University, London, UK, 1987.
[57] R.M.C. So, H.S. Zhang, C.G. Speziale, Near-wall modeling of the dissipation rate equation, AIAA J. 29 (1991) 2069–2076.
[58] C.G. Speziale, Analytical methods for the development of Reynolds-stress closures in turbulence, Annu. Rev. Fluid Mech. 23 (1991) 107–157.